

# Introducing a Physics-informed Deep Learning Framework for Bridge Scour Prediction

Negin Yousefpour, PhD, PE<sup>1</sup> and Bo Wang, PhD<sup>2</sup>

<sup>1</sup>Department of Infrastructure Engineering, The University of Melbourne. Email:  
negin.yousefpour@unimelb.edu.au

<sup>2</sup>Department of Infrastructure Engineering, The University of Melbourne. Email:  
bo.wang@unimelb.edu.au

## ABSTRACT

This paper introduces scour physics-informed neural network algorithms (SPINNs), a hybrid physics-data-driven framework for bridge scour prediction using deep learning developed based on historical scour monitoring data. SPINNs integrate physics-based empirical equations into neural networks as supplementary loss components. We examined three architectures: LSTM, CNN, and NLinear. While CNN and LSTM have shown competitive real-time scour forecasting in previous studies, NLinear with a simple architecture demonstrated the highest accuracy and significantly lower computational cost. Despite varying error reduction margins across different base models and bridges, SPINNs showed promising scour prediction and generally outperformed pure data-driven models. In some bridge cases, SPINN reduced forecasting errors by up to 50%. In this study, we also explored generalised models for bridge clusters by aggregating training datasets from multiple bridges in Alaska. Bridge/site-specific SPINNs incorporating HEC18 and time-dependent empirical equations provided more accurate predictions than SPINNs with generalised time-dependent equations. The three empirical equations derived from SPINN training in this study showed reasonable accuracy in estimating maximum scour depth. These deep learning derived empirical models can provide more accurate and reliable scour predictions than traditional HEC-18, particularly in scenarios lacking site-specific scour data. Comparing the HEC-18 model with both SPINNs and pure deep learning models highlights a substantial improvement in scour prediction accuracy, indicating a promising future for these hybrid machine learning methodologies for bridge scour design and maintenance.

# 1 Introduction

Scour is recognized as the leading cause of bridge failure in many countries. In the United States, scour is responsible for approximately 60% of bridge failures (Briaud J.L. et al., 2012). Historical data from other countries and regions, such as Australia, Taiwan, Japan, Germany, France, and Iran, shows that a large number of bridges have suffered scour-related failures due to typhoons and floods in the past few decades (Pizarro et al., 2020).

The complexity of predicting the expected maximum depth of scour at bridge piers stems from the intricate interactions between soil, hydrodynamic forces and the pier structure. Key challenges include uncertainties in riverbed material, flow conditions, geomorphological variations, and the increasing impacts of climate change. In recent decades, numerous research efforts have focused on developing empirical models to estimate scour depth using laboratory experiments and field observations. Despite these efforts, many empirical models tend to overestimate or underestimate scour depth due to their limited generalization across diverse riverbeds, flow, and structural conditions (Sheppard et al., 2011). For instance, the widely used HEC-18 scour equation, despite its evolution over the past two decades, has notable limitations, including insensitivity to various geological conditions, particularly to cohesive soils. Also, the empirical models are unable to provide a reliable assessment of scour variation with time and risk of scour failure, especially under flood conditions (Arneson et al., 2012). In response to this pressing need for more reliable predictive methods to enhance scour risk assessment and bridge safety, various Artificial Intelligence (AI) and Machine Learning (ML) methods have been explored. Readers are referred to Yousefpour et al. (2021), Yousefpour and Correa (2023), Hashem and Yousefpour (2024), and the cited references for a full literature review.

The ML models have been shown to outperform traditional empirical equations in estimating maximum scour depth. However, their performance remains restricted within the domain of training data and is highly dependent on the data quality and size, which are often scarce and do not cover a wide range of geological, hydraulic, and geomorphological conditions. In addition, these models are typically designed to predict the maximum scour depth for a given flow discharge and are not suitable for dynamic real-time forecasting. Given the limitations of current scour prediction models, bridge authorities have turned to monitoring solutions, including the use of continuous remote sensing systems enabling more reliable risk management for critical and large-scale bridges (NCHRP, 2009; Briaud et al., 2011). Pioneering works by Yousefpour et al. (2021), Yousefpour and Correa (2023), and Hashem and Yousefpour (2024) introduced deep learning (DL) solutions, specifically long-short-term memory (LSTM) networks and the convolutional neural network (CNN), for real-time scour forecasting. These models leverage LSTM and temporal CNN strength in temporal pattern recognition and capture the complex physical process of scour without direct feature extraction. By training on historical scour monitoring data, including time series of bed elevation, flow depth, and velocity, the DL models have shown the ability to predict upcoming scour depths up to a week in advance for case-study bridges in Alaska and Oregon.

Physics-based machine learning has accelerated as an emerging field in the past few years. The core idea is to incorporate physics law and constraints into the process of machine learning from data (Karpatne et al., 2017; Karniadakis et al., 2021). The hybrid physics-data-driven models have been introduced by a number of pioneering studies, referred to as physics-guided neural networks (PGNN) (Jia et al., 2021), physics-constrained neural networks (Raissi et al., 2019), and physics-informed neural networks (PINN) (Zhu et al., 2019). Although these terms have been alternately used in various recent studies (Faroughi et al., 2024). The incorporation of physical equations governing the response-input relationship, in the form of PDE/ODE

or closed-form models within the loss function, is being increasingly referred to as physics-informed ML; hence, in this study, we stick to this term. PINNs have been particularly developed to solve PDEs in application to various problems in solid mechanics (Haghigat et al., 2021), porous media simulations (Chen et al., 2023; Amini et al., 2023), constitutive modelling, and soil consolidation (Eghbalian et al., 2023; Li et al., 2024a; Lan et al., 2024; Tian and Wang, 2023; Masi and Einav, 2024). Likewise PGNNs have found successful applications in structural analysis (Yu et al., 2020; Chen and Liu, 2021), geohazard assessment (Pei et al., 2023; Zhang et al., 2020) tunneling (Li et al., 2024b), fluid mechanics (Yousif et al., 2022), among other fields.

Building on previously developed algorithms (Yousefpour and Correa, 2023; Hashem and Yousefpour, 2024), this paper introduces hybrid physics-data-driven models for scour prediction. A novel physics-informed deep learning framework is developed by integrating empirical scour models, based on the commonly used HEC-18 form, with prominent deep learning algorithms. We introduce SPINNs, *Scour Physics-Informed Neural Networks*, which leverage the temporal feature extraction capability of recurrent neural networks, convolutional neural networks, and feed-forward neural networks, while respecting the physics-based empirical equations. The models are trained using historical scour monitoring data from a number of case-study bridges in Alaska. As a by-product of the physics-informed deep learning models, data-driven empirical models are introduced for scour prediction. A comparison between the pure data-driven models and the hybrid physics-data-driven models shows that the physics-informed DL models result in more accurate predictions and far better generalisation compared with the DL models with no physics-based constraints. Moreover, unlike data-driven DL models, which have been bridge/site-specific, the physics-informed DL models can provide a generalisable hybrid physics-data-driven model that can provide more reliable predictions for any bridges when trained with sufficient data.

## 2 Approach

### 2.1 Notations and Definitions

To provide better clarity to our methodology, notations are provided in Table 1.

### 2.2 Scour Data and Preprocessing

The scour monitoring data of four bridges in Alaska is used to train the scour prediction models in this study. This data includes time series of river bed, measured by sonar sensors at the bridge pier, and flow elevations, measured by stage sensors or gauges at the upstream, as well as river discharge, estimated based on measurement of flow velocity using velocimeter or Acoustic Doppler sensors. This data was provided by the Alaska Department of Transportation (DOT) and the US Geological Survey (USGS).

Some of the missing data, for example, the discharge data was obtained from the Alaska Science Center online platform<sup>1</sup>. Most of the bridges on this platform contain the historical and real-time monitoring data collected from sonar and stage sensors attached to bridge piers with critical scour depth. The river discharge data in our methodology is only available for a few bridges at this point. Considering the data availability, we selected Bridge 212, 527, 539, and 742 with the key attributes presented in Table 2. The as-built bed elevation provides an important reference level to measure the scour depth. Pier and channel

<sup>1</sup><https://www.usgs.gov/centers/alaska-science-center/science/streambed-scour-bridges-alaska>

**Table 1.** Notations.

Symbol	Description	Unit
$t$	Timestep	hour
$E_{stage}$	Rive flow elevation measured by stage sensors at the upstream of the pier	m
$E_{bed}$	River bed elevation at the pier measured by Sonars	m
$E_{ref}$	Reference elevation for calculating local scour depth	m
$y_s$	Equilibrium scour depth	m
$y_{st}$	Time-dependent scour depth	m
$y_1$	Flow depth directly upstream of the pier	m
$M_{in}$	Input length (timesteps) of the NN	N/A
$M_{out}$	Output length (timesteps) of the NN	N/A
$Y_s$	Sequential forecasting targets contains observed scour depth values	N/A
$\hat{Y}$	The prediction on $Y_s$	N/A
$\hat{Y}_{sNN}$	The prediction on $Y_s$ by NN model	N/A
$\hat{Y}_{sPHY}$	The prediction on $Y_s$ by calibrated empirical equation	N/A
$a$	Pier width	m
$L$	Channel width	m
$V$	Mean velocity of flow directly upstream of the pier	m/s
$g$	Acceleration of gravity	9.81m/s <sup>2</sup>
$A$	Cross-sectional area of flow	m <sup>2</sup>
$q$	Average upstream discharge	m <sup>3</sup> /s
$K_1$	Correction factor for pier nose shape	N/A
$K_2$	Correction factor for angle of attack of flow	N/A
$K_3$	Correction factor for bed condition	N/A

dimensions are listed in meters. Also, coefficients  $K_1$ ,  $K_2$ , and  $K_3$  are factors used in the HEC-18 empirical equations as defined in Table 1.

This paper mainly follows the same preprocessing method outlined in [Yousefpour et al. \(2021\)](#) and [Yousefpour and Correa \(2023\)](#) for the historical bridge scour monitoring dataset. The raw data is aggregated on an hourly basis. The key preprocessing steps include outlier removal, smoothing and denoising, and linear imputation of missing data. The data availability of each monitored attribute is impacted by many factors, such as sensor reliability, seasonal river freezing, and flood occurrences. We synchronised  $E_{bed}$ ,  $E_{stage}$ , and  $q$ , ensuring the timesteps used for training the models include these three input features.

### 2.3 Scour Physics-Informed Deep Learning Framework

Over the past few decades, various physics(hydraulics)-based empirical equations have been developed to estimate local scour depth based on physical factors such as flow depth, flow velocity, pier geometry, and riverbed material/geology, calibrated based on laboratory and field testing ([Sheppard et al., 2011](#); [Arneson et al., 2012](#); [Kirby et al., 2015](#)). Our hypothesis here is that integrating such semi-empirical physics-based equations into machine learning can lead to more competent hybrid physics-data-driven models. These models can learn from historical scour data while respecting the underlying physics,

**Table 2.** Attributes of Case-Study Bridges.

No	Name	As-built	Channel	Pier	Pier	Attack	Pier	$K_1$	$K_2$	$K_3$
		Bed-Width	Width	Length	Angle	Nose	Shape			
212	Kashwitna River	48.8	65.2	1.5	8.5	0	Sharp	0.9	1	1.1
527	Salcha River	193.2	153.3	1.2	10.7	10	Round	1	1.8	1.1
539	Knik River	10.4	152.7	1.3	7.9	0	Sharp	0.9	1	1.1
742	Chilkat River	35.2	152.4	1.5	7.3	0	Round	1	1	1.1

potentially achieving superior generalization performance compared to pure data-driven ML models. This new framework can also lead to the development of more reliable data-driven empirical equations through machine learning optimization process.

We introduce Scour Physics-informed Neural Networks (SPINN) as a new physics-informed deep learning framework for scour prediction. This framework integrates an additional physical loss term into the objective function, guiding the deep learning models to learn from the specified empirical equation. The overall architecture of SPINN is depicted in Fig. 1.

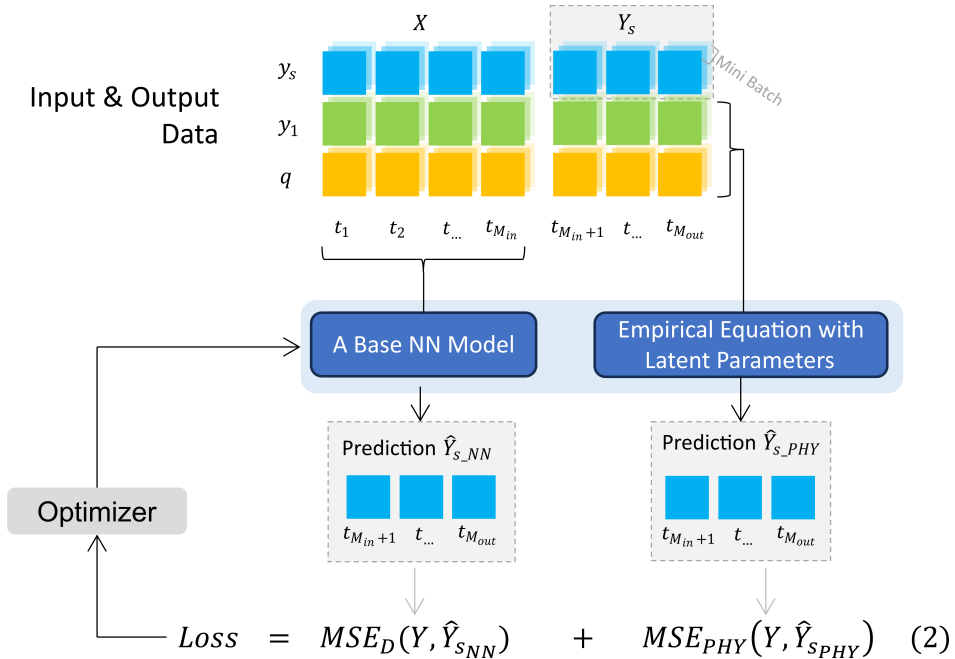


Fig. 1. SPINN framework, illustrating the integration of physics-based empirical equations as additional loss terms in the neural network training process.

The SPINN models are developed based on our pure data-driven LSTM and CNN scour forecast algorithms developed in Yousefpour and Correa (2023) and Hashem and Yousefpour (2024) for scour forecast based on historical sonar, stage, and discharge time series data. In addition, a simple DL linear architecture, NLinear is incorporated and compared with LSTM and CNN. The SPINN model processes

time series data as input and output, including scour depth,  $y_s$ , flow depth,  $y_1$ , and discharge,  $q$ . The input sequence  $X$ , contains these three features over  $M_{in}$  timesteps, while the output sequence,  $Y_s$  contains only scour depth,  $y_s$  over  $M_{out}$  timesteps. The discrepancy (loss) between the target (actual) scour depth ( $y_i$ ) and the predicted scour depth ( $\hat{y}_i$ ) is quantified using the Mean Squared Error (MSE) over the length of the output sequence. As opposed to pure data-driven ML, the objective function is defined as the sum of two loss terms, a data-driven loss ( $MSE_D$ ) and a physics-based loss ( $MSE_{PHY}$ ), as described in Equations 1 and 2:

$$MSE = \sum_{i=0}^{M_{out}} (y_i - \hat{y}_i)^2 \quad (1)$$

$$Loss = MSE_D(Y, \hat{Y}_{s_{NN}}) + MSE_{PHY}(Y, \hat{Y}_{s_{PHY}}) \quad (2)$$

Within this framework,  $\hat{Y}_{s_{NN}}$  represents the output from the base NN model (pure ML), and  $\hat{Y}_{s_{PHY}}$  denotes the predictions yielded by the empirical equation (calibrated through ML training). For this purpose, the  $y_1$  and  $q$  within the output timesteps ( $M_{out}$ ) are used as input data for the physics empirical equation. By concurrently optimizing these two loss components, the SPINN model is supposed to achieve better predictive accuracy and generalizability.

In this study, we implement three SPINN variants, tailored by different forms of the empirical equations, ranging from widely accepted equations to a highly generalized form as described in the following sections. These equations involve latent parameters calibrated based on time series data throughout the training process. These parameters are optimized by Adam optimizer based on the total loss alongside the hidden parameters of the base NN model (Kingma and Ba, 2014).

### 2.3.1 SPINN with HEC18 Equation (SPINN-HEC18)

HEC-18, officially known as Hydraulic Engineering Circular No. 18, is a widely recognized engineering guideline published by the United States Federal Highway Administration (FHWA). This guideline provides recommendations on maximum scour depth prediction. Over time, HEC-18 has undergone iterative revisions, with the most current version documented in Arneson et al. (2012). The latest HEC-18 Equation (3) is shown in Equation (3):

$$y_s = 2.0aK_1K_2K_3\left(\frac{y_1}{a}\right)^{0.35}\left(\frac{V}{gy_1^{0.5}}\right)^{0.65} \quad (3)$$

where  $y_s$  is the equilibrium scour depth,  $y_1$  is the flow depth,  $a$  is the pier width, and  $K_1$ ,  $K_2$ ,  $K_3$ , are correction factors related to flow and pier as defined in Table 1. This equation is normally calibrated using datasets from field and laboratory measurements. These measurements represent different bridges with distinct scour characteristics. Unlike time series data, they are discretely collected, based on snapshots of scour conditions at different times and locations.

In this paper, we use the time series data collected from continuous real-time sensor measurements on bridge piers, including riverbed elevation, flow elevation and discharge,  $E_{bed}$ ,  $E_{stage}$ , and  $q$ . Therefore,  $y_s$  and  $y_1$  at each timestep can be derived by the following equations as shown in Fig. 2a:

$$y_1 = E_{stage} - E_{ref} \quad (4)$$

$$y_s = E_{ref} - E_{bed} \quad (5)$$

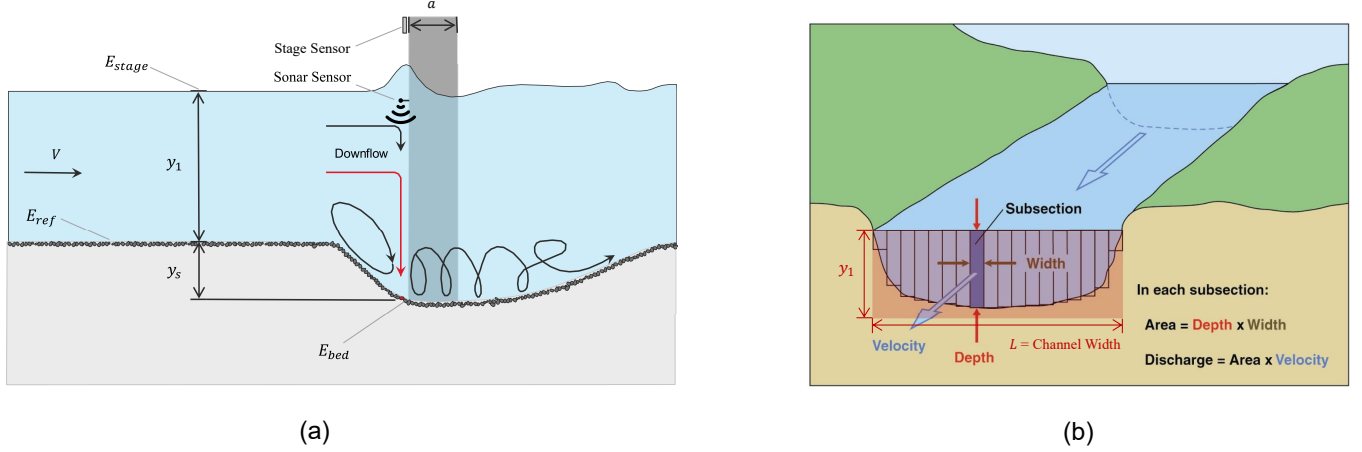


Fig. 2. a) Profile of pier subjected to scour, showing sensors and variables [adapted from Arneson et al. (2012)], b) Calculation of channel cross-sectional area and the relationship between velocity and discharge.

where  $E_{stage}$  is the stage (elevation of the flow directly upstream of the pier),  $E_{bed}$  is the bed elevation, and  $E_{ref}$  is the reference level. For SPINN-HEC18, we use the as-built bed elevation as  $E_{ref}$ .

We derive average velocity ( $V$ ) based on the time series of discharge data ( $q$ ), as the direct measurements of velocity are not provided by USGS. As shown in Fig. 2b, discharge can be estimated by river channel cross-sectional area times velocity. The cross-sectional area of flow ( $A$ ) is not easy to measure nor available in this study, therefore we assume that  $A$  can be calculated as  $y_1 \times L$  multiplied by a fixed ratio  $p_2 \in [0, 1]$ , which can be estimated as a latent parameter within SPINN. Therefore,  $V$  can be calculated as:

$$V = \frac{q}{A} = \frac{q}{p_2 L y_1} \quad (6)$$

In addition, we include  $p_1 \in [-1, 1]$  as another latent parameter adjusting the river and flow correction factor. Therefore, the empirical equation,  $\hat{Y}_{SPHY}$  can be written as:

$$\hat{Y}_{SPHY} = p_1 2.0 K_1 K_2 K_3 \frac{a^{0.65}}{g^{0.215} L^{0.43} y_1^{0.295}} \left( \frac{q}{p_2} \right)^{0.43} \quad (7)$$

where  $p_1$  and  $p_2$  will be calibrated through the SPINN training process, resulting in a new calibrated empirical equation.

Equation 7 is only applicable during scouring episodes and not to filling episodes. To account for this, we impose a condition to include the physical loss term in the total loss only when  $y_s$  is greater than zero (i.e.,  $E_{ref} > E_{bed}$ ). When  $y_s$  becomes negative, which happens during filling episodes, the  $MSE_{PHY}$  term is set to zero for those specific mini-batches or sequences.

### 2.3.2 SPINN with Time-Dependent HEC18 Equation (SPINN-TD)

Our dataset records show that the Alaskan bridges experience live-bed scour, where the riverbed goes through iterative cycles of scouring and filling (Ngo, 2018). For each occurrence of a scour event, the progression of live-bed scour can be outlined into two distinct phases, as illustrated in Fig. 3a. In the initial growth phase, local scour initiates from a depth of zero and gradually deepens. Upon reaching equilibrium depth, the local scour undergoes fluctuations, maintaining a relatively steady state. During

this balanced phase, the flow dynamics lead to sediment deposition and erosion, resulting in a state of equilibrium. Furthermore, in the balanced phase, both upper and lower bounds of the scour depth become apparent. Consequently, various time-dependent equations (Sheppard et al., 2011; Liang et al., 2019) have been developed to approximate the upper bound of scour depth, as depicted in Fig. 3b.

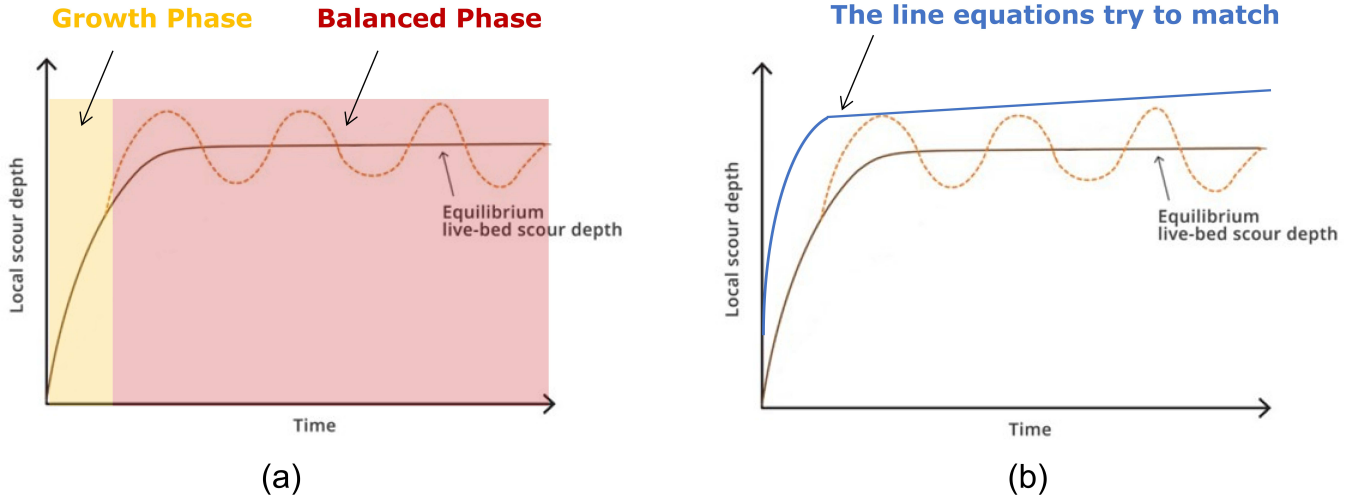


Fig. 3. Temporal features of live-bed local scour: a) Different phases of scour evolution, b) The ideal fitting line representing the upper bound of scour depth. Source: Ngo (2018).

We define a time-dependent scour empirical model based on the maximum local scour depth equation of ( $y_{s\_max}$ ) HEC18 and an exponential form to account for time-dependency as shown in Equation 8. During a scouring episode, the last timestep  $M_{out}$  within the target sequence is considered close to the maximum scour depth in that episode, and the values of  $y_{1\_max}$  and  $q_{max}$  are derived from this timestep.

$$\hat{y}_{st} = y_{s_{max}} \left( 1 - e^{-\frac{p_3 \times t}{T_L}} \right) = p_1 2.0 K_1 K_2 K_3 \frac{a^{0.65}}{g^{0.215} L^{0.43} y_{1\_max}^{0.295}} \left( \frac{q_{max}}{p_2} \right)^{0.43} \left( 1 - e^{-\frac{p_3 \times t}{T_L}} \right) \quad (8)$$

In this equation,  $\hat{y}_{st}$  is the predicted time-dependent local scour depth at timestep  $t$ , where  $t \in \{0, 1, 2, \dots, M_{out} - 1\}$  represents the time steps of the output sequence.  $T_L$  is the time lag between the maximum scour depth and the maximum flow, which is often observed in the scour process. This time lag is physically meaningful as it accounts for the delayed response of the scour depth to the flow conditions.  $p_1$ ,  $p_2$ , and  $p_3$  are latent parameters, where  $p_3$  represents the decay rate in the exponential function, controlling how quickly the scour depth approaches the equilibrium state. These parameters are passed through a hyperbolic tangent (tanh) activation function, which constrains their values to the range  $[-1, 1]$ .  $T_L$  is set to be within the range  $[0, 2 \times (M_{in} + M_{out})]$ . By setting the upper limit of  $T_L$  to be twice the sum of  $M_{in}$  and  $M_{out}$ , we ensure that the parameter has sufficient flexibility to learn the appropriate time lag between the maximum scour depth and the maximum flow, even if the lag extends beyond the output sequence length. To fit different scouring events throughout the time series, we consider the elevation in the first timestep of each training pair as  $E_{ref}$ , which is dynamically updated for different input and output data pairs.

Given that the time-dependent equation mentioned above is specifically applicable to instances of scouring episodes, it is important to identify these episodes as illustrated in Fig. 4. The training workflow for a single data batch comprises several key steps. Initially, the bed elevation values of the first timestep

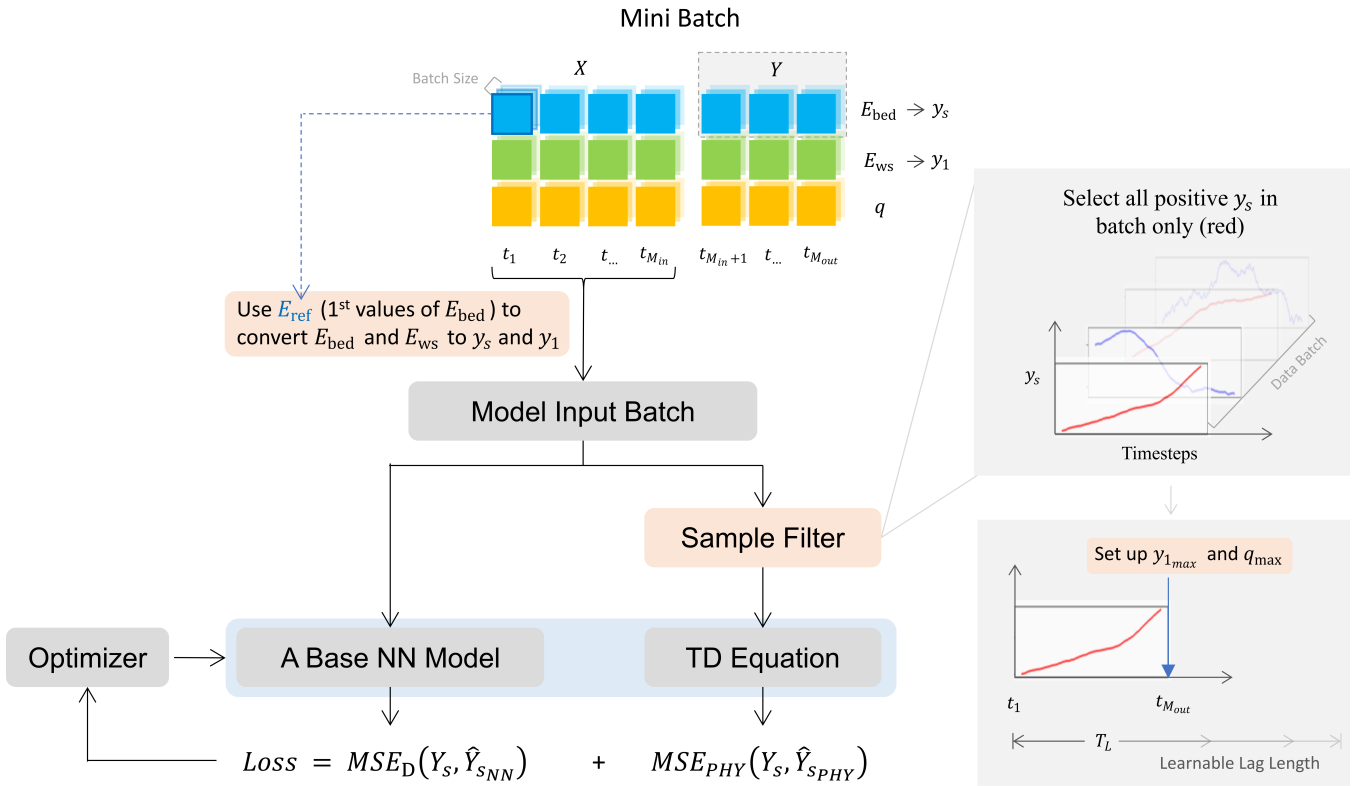


Fig. 4. The training process of the time-dependent SPINN model, which incorporates scouring episode detection and applies the physical loss term only during scouring episodes.

within the mini-batch are picked as the reference level  $E_{ref}$  for calculating flow depth and scour depth for each sequence, which are inputs for the NN model and the TD empirical equation. During this process, the sequences pass through the conditional term ( $MSE_{PHY}$ ) to filter scour episodes, similar to SPINN-HEC18 models. The physics loss and Equation 8 are only applied to the scour episodes (i.e., positive scour depths).

Similar to SPINN-HEC 18, the training is performed based on total loss for all mini-batches, including both scouring and filling episodes, to adjust the hidden parameters in the NN model and latent parameters in the TD empirical equation. The  $MSE_{PHY}$  term is set to zero for filling episodes/sequences.

### 2.3.3 General Time-Dependent Equation (SPINN-GTD)

SPINN-TD model has indeed incorporated the use of a time-dependent equation; however, it is important to note that using this equation requires an abundance of site-specific data, including pier geometry, pier shape, channel width, correction factors for bed condition, and flow attack angle. In order to develop a general model that does not require site-specific information, we introduce SPINN-GTD by eliminating all site-specific parameters from the empirical equation in the SPINN-TD (Equation 9), as outlined in Equation 9.

$$\hat{y}_{st} = p_1 (y_{1max})^\alpha \left( \frac{q_{max}}{p_2} \right)^\beta \left( 1 - e^{-\frac{t}{T_L}} \right) \quad (9)$$

where  $\alpha$  and  $\beta$  represent hyperparameters introduced to offer more flexibility in the shape of the

empirical model to adjust to a range of bridges.

This approach enables the model to learn the features of a wider range of scour events in various bridges with different scour conditions, enhancing predictive accuracy and generalisation of the SPINN model to new bridge scour cases. Likewise, the generalised time-dependent equation calibrated through this SPINN model can potentially provide more accurate maximum scour depth predictions across a wide range of bridges and scour conditions.

### 2.3.4 Long Short-Term Memory Networks (LSTM)

LSTM is a type of recurrent neural network (RNN) that excels in capturing and modelling temporal dependencies within time series/sequential data (Hochreiter and Schmidhuber, 1997). A critical challenge in training deep neural networks is the vanishing gradient problem, where gradients shrink to a very small level during back-propagation, which hinders effective learning. LSTM networks address this problem through their unique gate mechanisms, which regulate and maintain the gradient flow, preventing its significant diminish across the network's layers. The strength of LSTMs lies in their ability to remember long-term dependencies in sequential data, allowing them to capture complex patterns that traditional models might miss. This feature is particularly advantageous in time series prediction, where future outcomes are influenced not just by recent events but also by occurrences in the distant past, resulting in more accurate and robust predictions.

In this study, we implement a one-layer LSTM model with 128 hidden units as shown in Fig. 5. The input sequence is processed by the LSTM layer and then passed through a dense (fully connected) layer with a linear activation function and eventually reshaped into the output sequence.

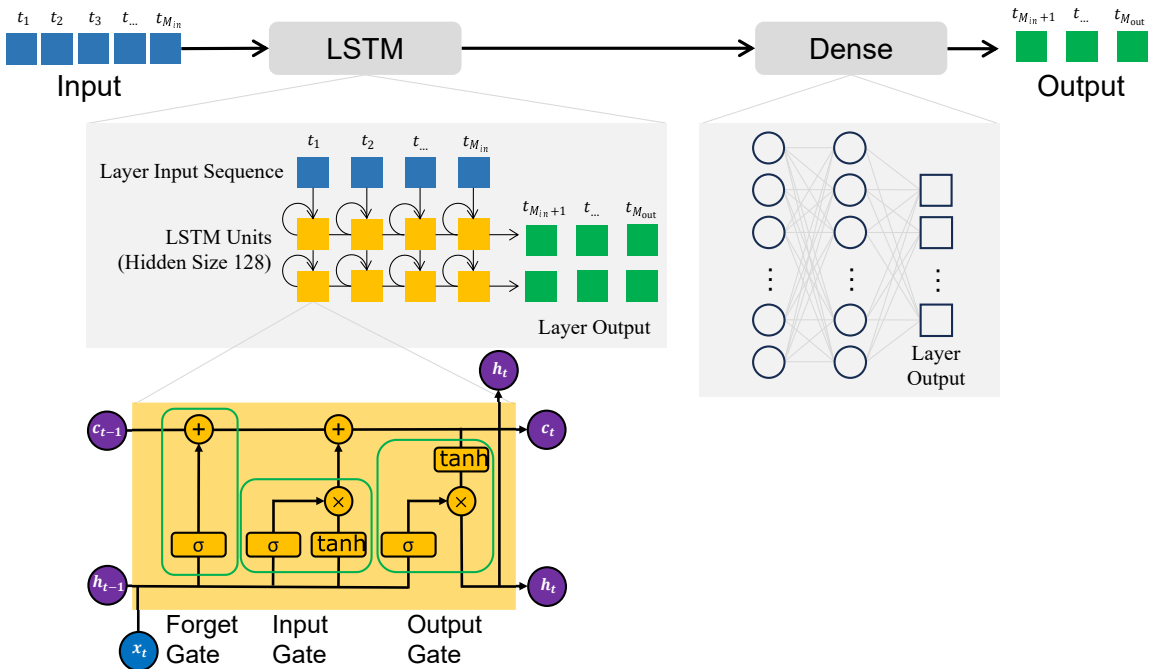


Fig. 5. The architecture of LSTM model. An LSTM Memory Unit below showcasing the input ( $x_t$ ), hidden ( $h_t$ ), and cell state ( $c_t$ ) vectors, with gates (forget, input, and output) that dynamically regulate the flow of information through the unit to maintain and update the memory.

### 2.3.5 Convolutional Neural Network (CNN)

CNN is one of the most prevalent types of neural network applied in computer vision due to its effectiveness in learning image features (Venkatesan and Li, 2017). In recent years, they have also found applications in time series prediction tasks, where the inputs are structured as sequential data (Livieris et al., 2020). Similar to spatial pattern identification in images, CNN can also be adapted to capture temporal patterns and dependencies within sequential data in the context of time series prediction (Liu et al., 2022).

In this study, we develop a CNN model with two 2D convolutional layers to show the adaptability of CNNs for processing multidimensional time series data. The two CNN layers have a kernel size of 5, padding size of 2, and output sizes of 128 and 256, respectively. Also, batch normalization layers are added after these layers, and one following dense layer is responsible for producing the final prediction.

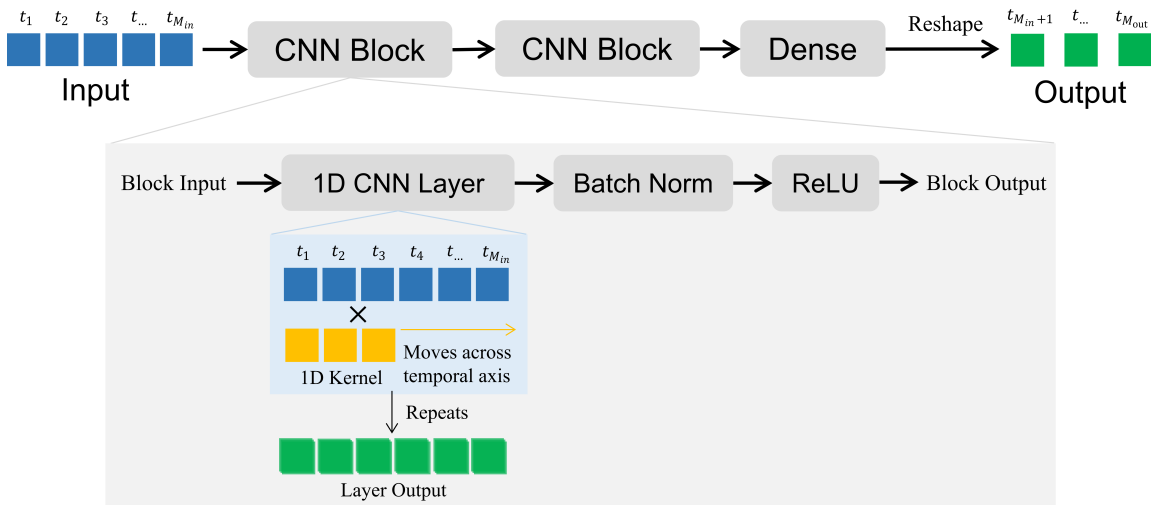


Fig. 6. The architecture of CNN model.

### 2.3.6 NLinear

The NLinear neural network is a variant within the Long-term Time Series Forecasting Linear (LTSF-Linear) framework proposed by Zeng et al. (2023), which uses only one dense layer to model multi-step time series forecasting problems. Notably, this variant is designed to improve the performance in the presence of distributional shifts of temporal data. This phenomenon refers to the temporal fluctuations in data properties caused by various factors, such as seasonal patterns and short-term trends, which reduces the generalization ability of predictive models trained on past observations. The NLinear model (see Fig. 7) mitigates distribution shifts by centring the input sequence around its last value, both before and after the linear transformation. It subtracts the last value from the sequence, processes it through a dense layer, and then re-adds that value to the output, thus maintaining the original data distribution.

Although the NLinear structure is simple and contains only one layer, it has been shown by several studies to outperform more complicated transformer-family models designed for multi-step time series prediction, such as Transformer (Vaswani et al., 2017), Informer (Zhou et al., 2021), and FedFormer (Zhou et al., 2022).

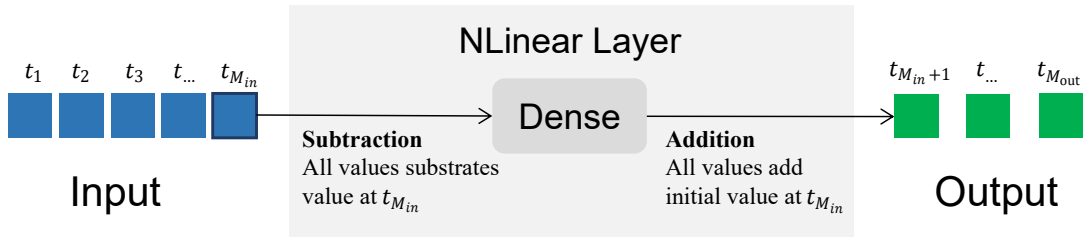


Fig. 7. The architecture of NLinear model.

### 3 Results and Discussion

#### 3.1 Model Configuration and Experimental Design

To validate the efficacy of the SPINN framework, a series of experiments are proposed in this section. The detailed model configuration and comparison experiments are introduced as follows.

##### 3.1.1 Model Configuration and Training Data

Based on the top model configurations identified through comprehensive hyperparameter tuning performed in [Hashem and Yousefpour \(2024\)](#), the  $M_{in}$  and  $M_{out}$  for all models are set to 168 timesteps, equivalent to seven days. This means that after training the models with the historical time series data up to the current time, the last one-week data is used as input to predict the scour depth for the coming week. Fig. 8 shows the historical time series data of Bridge 539 as an example. Multiple data gaps are found within the data, which is mainly due to sensor malfunctions or seasonal freezing in Alaska.

We use a sliding window with a length equal to  $M_{in}$  plus  $M_{out}$  to slice the data into the sequences for training. The range of available time series data and the number of available sequences over training and test datasets in each bridge is provided in Table 3.

**Table 3.** The split of training, validation, and testing sets for each bridge.

Bridges	Type	Start	End	No. of Sequences
212	Train/Validation	2012-06-05 13:00	2017-08-06 02:00	11,573
212	Test	2017-08-06 03:00	2018-09-27 03:00	2725
527	Train/Validation	2005-06-02 15:00	2019-06-11 11:00	41,473
527	Test	2019-06-11 12:00	2021-09-25 22:00	9782
539	Train/Validation	2003-05-13 17:00	2019-07-10 17:00	29,626
539	Test	2019-07-10 18:00	2021-09-25 20:00	7155
742	Train/Validation	2013-05-27 02:00	2017-07-09 23:00	7,462
742	Test	2017-07-10 00:00	2017-09-11 17:00	1,530

For each bridge, we have multiple time series data across years. Once the input and output sequence lengths are determined, we create input-output pairs by sliding a window over the continuous time series

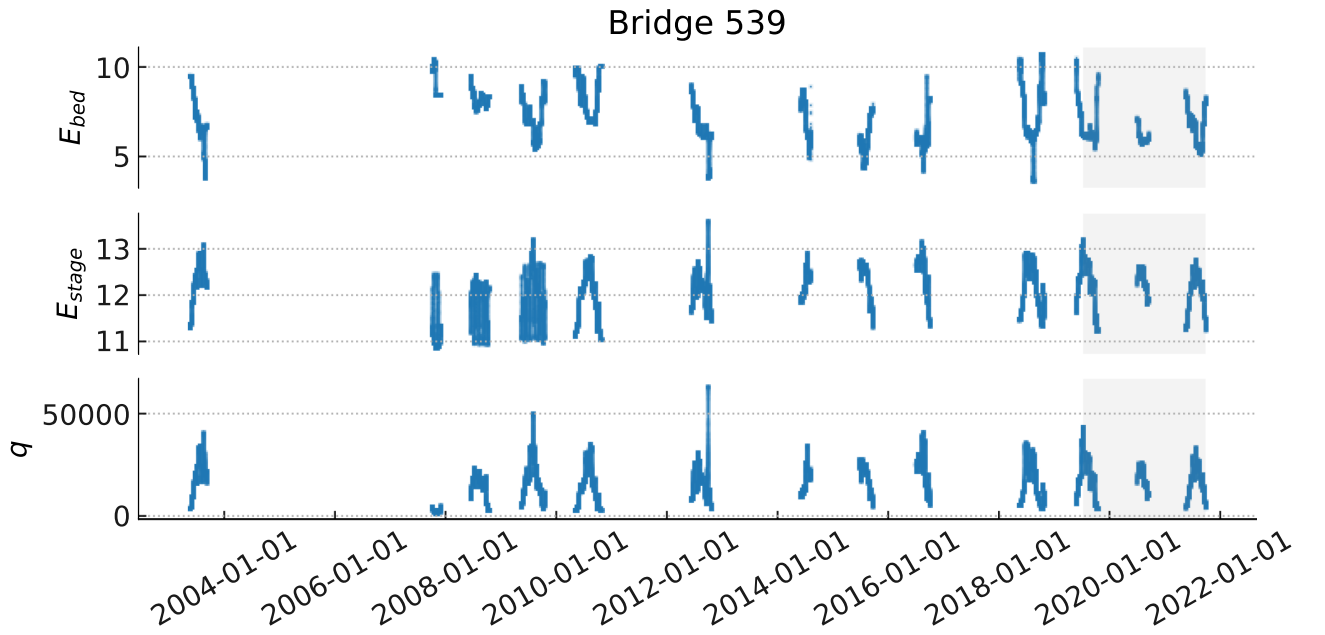


Fig. 8. Historical time series data for Bridge 539 shows the three features: bed elevation ( $m$ ), river stage elevation ( $m$ ), and discharge ( $m^3/s$ ). The grey zone shows the test subset, and the transparent part before is the training and validation subsets.

data, resulting in a set of available samples. We arrange these samples in temporal order and allocate the last 20% for the test set. The first 80% of the samples are then randomly split into training and validation sets in a 3:1 ratio (60% for training and 20% for validation). The model is validated after each training epoch to monitor its performance on unseen data and prevent overfitting. Fig. 8 illustrates the data split for Bridge 539. Similar illustrations for other bridges can be found in the Appendix Section (Figs. A1 to A3).

### 3.1.2 Experimental Design

A number of experiments were performed to evaluate the performance of the three SPINN variants and their counterpart pure NN (base data-driven) models. The experiments can be categorized into general and site/bridge-specific as shown in Table 4.

The models trained using bridge-specific data will be evaluated with the corresponding test set, while the model trained on all bridges will be evaluated individually for each of the four bridges. Considering the stochastic nature inherent in NN modelling, each experiment is trained and evaluated five times to ensure the robustness of results. The averaged MSE over the validation and test datasets are used to evaluate the performance of models.

In addition to MSE, we also use Mean Absolute Percentage Error (MAPE) and Root Mean Squared Error (RMSE) as performance metrics to evaluate the models. MAPE and RMSE are defined as:

$$MAPE = \frac{1}{M_{out}} \sum_{i=0}^{M_{out}} \left| \frac{y_i - \hat{y}_i}{y_i} \right| \times 100 \quad (10)$$

**Table 4.** Experiment design for evaluation of SPINN variants and their corresponding pure data-driven models. The general models trained using a combination of all four datasets indicated as "All". The latent parameters calibrated through the SPINN training process are highlighted.

Experiments	Training Base	$\hat{Y}_{SPHY}$
	Dataset	Data-Driven Model
Pure NN (Site-Specific)	212 527 539 742	LSTM CNN NLinear
Pure NN (General)	All	LSTM CNN NLinear
SPINN-HEC18 (Site-Specific)	212 527 539 742	LSTM $\textcolor{magenta}{p_1} 2.0 K_1 K_2 K_3 \frac{a^{0.65}}{g^{0.215} L^{0.43} y_1^{0.295}} \left( \frac{q}{\textcolor{magenta}{p_2}} \right)^{0.43}$ CNN NLinear
SPINN-TD (Site-Specific)	212 527 539 742	LSTM $\textcolor{magenta}{p_1} 2.0 K_1 K_2 K_3 \frac{a^{0.65}}{g^{0.215} L^{0.43} y_{1\max}^{0.295}} \left( \frac{q_{\max}}{\textcolor{magenta}{p_2}} \right)^{0.43} \left( 1 - e^{-\frac{\textcolor{magenta}{p_3} \times t}{\textcolor{magenta}{T_L}}} \right)$ CNN NLinear
SPINN-GTD (General)	All	LSTM $\textcolor{magenta}{p_1} (y_{1\max})^{\textcolor{magenta}{a}} \left( \frac{q_{\max}}{p_2} \right)^{\textcolor{magenta}{b}} \left( 1 - e^{-\frac{t}{\textcolor{magenta}{T_L}}} \right)$ CNN NLinear

$$RMSE = \sqrt{\frac{1}{M_{out}} \sum_{i=0}^{M_{out}} (y_i - \hat{y}_i)^2} \quad (11)$$

where  $y_i$  is the actual scour depth and  $\hat{y}_i$  is the predicted scour depth at timestep  $i$ .

The models were implemented using PyTorch (Paszke et al., 2017) python packages and were run on 4 NVIDIA A100 Tensor Core GPUs and 2×16 Core CPUs on the *Geo&Co* Infrastructure Department High-Performance Computing Center at the University of Melbourne.

### 3.2 Performance Assessment

Fig. 9 presents the performance distribution for all models over the test dataset. The detailed results of experiments are listed in Table A1. The aggregated MSE of five runs are listed as mean and standard deviation values for each model. In the following subsections, we will discuss the main findings of these experiments.

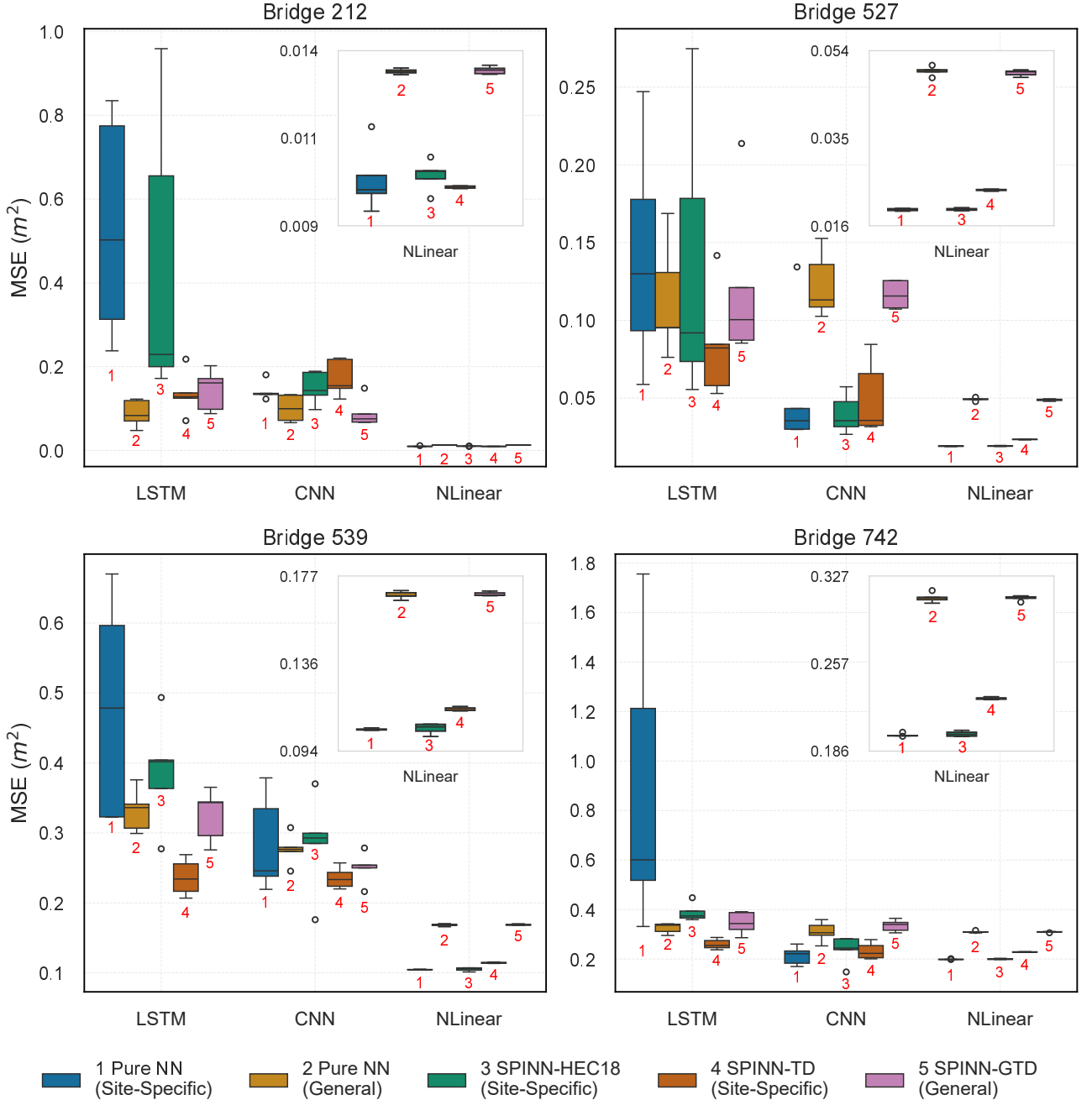


Fig. 9. Comprehensive analysis of model performance across four bridges, showing the test MSE ( $m^2$ ) distribution for pure NN models and SPINN variations. The right-top in each subplot shows the zoom-in area of the NLinear group due to their smaller scales.

### 3.2.1 Site-Specific and General Pure Data-Driven Models

Analysing the predictive performance across bridges among site-specific and general models is crucial before investigating the impacts of NN algorithms. As observed in Fig. 8, and also Fig. A1 to A3, there are significant fluctuations in the bed elevation  $E_{bed}$  across the bridges. For instance, Bridge 539

experienced several significant scour events across the years, with some scour depths reaching over five meters. In contrast, the  $E_{bed}$  changes at Bridge 527 were relatively modest, with variations consistently below two meters. Such differences are caused by distinct riverbed material geology, geomorphology, river flow characteristics, and bridge design. All of these various factors can have an impact on the scouring processes and result in predictive complexities.

**Table 5.** Performance of pure data-driven models trained on site-specific and general datasets, based on MSE ( $m^2$ ) / MAPE (%) values. Elev. represents the maximum bed elevation variation ( $m$ ) over the test dataset.

	Elev.	Pure-LSTM		Pure-CNN		Pure-NLinear	
		Site-Specific	General	Site-Specific	General	Site-Specific	General
212	0.644	0.533/0.069	0.089/0.034	0.142/0.041	0.101/0.033	0.010/0.014	0.013/0.016
527	2.030	0.141/0.010	0.113/0.010	0.055/0.006	0.123/0.010	0.019/0.004	0.049/0.006
539	4.603	0.478/0.537	0.332/0.546	0.283/0.406	0.276/0.485	0.105/0.250	0.168/0.358
742	3.191	0.884/0.127	0.325/0.111	0.214/0.079	0.310/0.106	0.199/0.076	0.310/0.102

The performance measures presented in Table 5 and Fig. 9 reveal that the relative performance of different NN models varies across bridges. MAPE and MSE criteria indicate different orders of performance for the bridges. Based on the average MAPE values across all models, the order of bridges from lowest to highest MAPE is 527, 212, 742, and 539. In contrast, the order of bridges based on average MSE values from lowest to highest is 212, 527, 539, and 742. These different orderings highlight the importance of considering both MAPE and MSE when evaluating model performance across different bridges, as they capture different aspects of prediction accuracy. MAPE is a percentage-based metric that provides insights into the relative magnitude of errors and is particularly useful when comparing models across bridges with varying scales of bed elevations. On the other hand, MSE concentrates larger errors by squaring them, making it more sensitive to outliers. By considering both MAPE and MSE, we can gain a more comprehensive understanding of the model performance. The trend in model performance does not show a correlation with the amount of training data available for each bridge (see Table 3) and can be pertained to various complex factors such as quality of data, scale of variation, amount of missing data, and consistency in seasonal and temporal patterns across years. Nevertheless, these experiments indicate that the bridges with smaller range/scale of variation and fluctuations of bed elevation seem to achieve better prediction performance overall with both MAPE and MSE criteria.

For the general data-driven models (Pure NN-General), we used the collective dataset from all bridges for their training and then evaluated the model for each bridge scour forecasting individually. The interesting outcome is that the general models yielded better and more stable performance (lower MSE and lower standard deviation) compared to site-specific for the majority of models, except for CNN in the case of Bridge 212 and 539 (see Table 5 and Fig. 9). For instance, training the LSTM model with the combined datasets from all bridges led to 63% and 83% reduction in MSE for bridges 742 and 212, respectively, compared to site-specific LSTM models trained with local data only. These two bridges had specifically less amount of site-specific data, which indicates how a larger dataset, even across different bridges, can enhance the generalization of pure NN models. This outcome highlights the potential for developing accurate global scour forecast models applicable to a cluster of bridges in a region.

While general models in this case study proved superior to bridge/site-specific models, the unique

scour characteristics of other bridges may still demand the development of site-specific models to achieve optimal results.

### 3.2.2 SPINNs and Choice of Physics-based Empirical Equation

The integration of physics-based loss components into NN models, including HEC18, TD, and GTD equations, has led to improvement in predictive accuracy in most of the bridges as observed from Fig. 9 and Table 6. Considering all bridges and base models (represented by the five colours within each group in the figure), the SPINN-based methods consistently achieve the lowest MSE value within their respective groups in most cases, demonstrating their superior performance compared to the pure NN models. For instance, all three SPINN variants have achieved lower MSEs in the LSTM group of Bridge 212. Furthermore, in the LSTM group of Bridge 539, the SPINN-TD helped to reduce the MSE from 0.478 to 0.236 (50.63% error reduction). The reference level ( $E_{ref}$ ) for scour depth calculations differs among SPINN variants: SPINN-HEC18 uses the constant as-built bed elevation, while SPINN-TD and SPINN-GTD employ a dynamic approach, updating  $E_{ref}$  based on the bed elevation of the first timestep in each input-output sequence pair.

**Table 6.** Performance of SPINN variants across different bridges, based on MSE ( $m^2$ ) values. Elev. represents the maximum bed elevation variation ( $m$ ) over the test dataset.

Elev.	SPINN-HEC18			SPINN-TD			SPINN-GTD			
	LSTM	CNN	NLinear	LSTM	CNN	NLinear	LSTM	CNN	NLinear	
212	0.644	0.443	0.150	0.010	0.136	0.173	0.010	0.144	0.089	0.013
527	2.030	0.135	0.040	0.019	0.084	0.050	0.023	0.122	0.130	0.049
539	4.603	0.388	0.285	0.105	0.236	0.236	0.114	0.325	0.250	0.169
742	3.191	0.388	0.239	0.200	0.260	0.233	0.229	0.346	0.335	0.310

Table 6 provides a comprehensive comparison of the performance of different SPINN variants across the case study bridges. The SPINN-TD model consistently outperforms the other SPINN variants, achieving the lowest MSE for most of the bridges when paired with LSTM and CNN base models. This suggests that incorporating the proposed site-specific time-dependent equation (TD) as a physics-based loss function is more effective compared to the site-specific HEC18 and the generalized version of the TD equation (GTD). However, the degree of performance improvement varies depending on the specific bridge and base NN model. For instance, while SPINN-TD shows significant error reduction for Bridge 539 when paired with LSTM (50.63% reduction) and CNN (16.61% reduction), the improvement is less pronounced for Bridge 527 with the same base models (40.43% and 9.09% reduction, respectively). This variability in performance gain suggests that the effectiveness of the physics-based loss functions is influenced by the inherent characteristics of each bridge dataset.

Among the different base DL models, LSTM, followed by CNN, seems to achieve the most performance improvement in terms of accuracy (error) and robustness (variance) from a physics-informed architecture. It is noted that the NLinear model does not show a significant benefit from adding the physics loss to its architecture in any form.

### 3.2.3 Effect of Base DL Algorithm on SPINNs

This paper employs LSTM, CNN, and NLinear as the base models. A comparative analysis of their trainable parameters and computational intensity, expressed in terms of Floating Point Operations (FLOPs), is presented in Table 7. The number of trainable parameters reflects the model’s capacity to learn from data, while FLOPs provide insight into the computational demands of processing that data. In deep learning, FLOPs are estimated by counting the total number of multiplication and addition operations required for one forward pass through the model.

**Table 7.** Latent Parameters and FLOPs for Different Models.

Model	Trainable Parameters	FLOPs
LSTM	3,681,448	22,966,272
CNN	7,393,704	42,513,408
NLinear	28,392	56,448

As shown in Table 7, there is a direct correlation between the model’s complexity and its computational cost. The CNN architecture requires approximately twice the computational effort of the LSTM due to its complex convolutional layers. In contrast, the NLinear model demands significantly fewer resources—only about 0.77% of the FLOPs required for LSTM operations. Regarding the SPINN framework, HEC18, TD, and GTD only introduce a few latent parameters to the base NN (See Table 4, thereby leading to a negligible extra computational cost. This enables SPINN variants to leverage the benefits of physics-informed learning without incurring a substantial computational burden.

Across the bridges analyzed in this research, the models founded on the NLinear consistently outperform the LSTM and CNN in terms of average MSE values. Considering the relatively small computational cost, NLinear works more efficiently compared to others. The potential reason behind this phenomenon has been unveiled by the authors of NLinear (Zeng et al., 2023). According to their experiments on various time series datasets, it has been found that linear models can be more effective in certain scenarios where there are clear trends and periodicity in the data. This is due to their simplicity and direct approach to handling time series data.

However, it is important to acknowledge that bridge-scouring events are a complex process. While NLinear models offer considerable advantages, a comprehensive modelling approach should not disregard the potential utility of other NN architectures. Different NN structures may provide unique insights or afford better performance under diverse conditions. When modelling a wider range of scenarios, multiple NN structures should be considered as baselines.

### 3.2.4 General DL Models for Bridge Clusters

In this study, we implemented Pure NN (All) and SPINN-GTD experimental groups to assess general DL models that can provide reasonable forecast accuracy across a cluster of bridges (such as our selected four case-study bridges in Alaska). General models can significantly reduce development and computational costs by eliminating the need for site-specific models (i.e., individual bridge models). As discussed in Section 3.2.1, the general data-driven models outperformed the site-specific data-driven models; however, as observed in Fig. 9, the general hybrid physics-data-driven models (SPINN-GTD) did not show superiority

to site-specific physics-data-driven variants, i.e. SPINN-HEC18 (except for LSTM-539, LSTM-742, CNN-212) and SPINN-TD (except for CNN-212).

The challenge in generalization arises from the diverse riverbed, flow and pier geometry across different bridges. The GTD equation is designed to capture a broad range of scour behaviour within a single equation by combining multiple bridge-specific coefficients, i.e.,  $K_1$ ,  $K_2$ ,  $K_3$ , and  $a$  into one latent parameter  $p_3$ . When incorporating GTD as the physical loss, the equation could potentially limit the NN's ability to adequately learn and adapt to the specific scouring patterns inherent to each bridge, leading to a degradation in prediction accuracy. Therefore, a more nuanced approach involving bridge-specific adaptations (such as coefficients used in HEC18 and TD), might be necessary to help improve NN learning.

### 3.3 Forecasting Trends and Capturing Scour Events

The primary objective of the scour forecasting model lies in its ability to predict major scour events in advance. Fig. 10 and Fig. 11 present the SPINN model prediction over the test dataset by the three SPINN models. Due to relatively stable bed elevation in the test sets of Bridge 212 and 527, our analysis here is focused on Bridges 539 and 742. The actual river bed elevation changes are depicted as a solid brown line, while the model predictions are shown as dashed lines. The predictions using pure NN models and the calibrated HEC18 empirical equation (CEE-SPINN-HEC18) derived from SPINN, as discussed in Section 3.4, are used as baselines for comparison. The magnified subplots in Fig. 10 and Fig. 11 highlight the analysis of major scour events on Bridges 539 and 742. The major scour event at bridges 539 and 742 occurs in July with a maximum depth of 1.5 and 1.4 meters, respectively. Table 8 compares the RMSE in maximum scour depth prediction for these two major events.

**Table 8.** Prediction error over the main scour events of Bridges 539 and 742. RMSEs ( $m$ ) are computed between the starting and ending timesteps of the major scouring events in their test sets. Bold values highlight the improved prediction of SPINN compared to Pure NN.

Model	Training Datasets	Method	RMSE - 539	RMSE - 742
LSTM	Site Specific	Pure NN	$0.506 \pm 0.057$	$0.289 \pm 0.011$
LSTM	Site Specific	SPINN-HEC18	$0.509 \pm 0.063$	$0.292 \pm 0.022$
LSTM	Site Specific	SPINN-TD	$0.514 \pm 0.025$	<b><math>0.264 \pm 0.012</math></b>
LSTM	General	Pure NN	$0.657 \pm 0.070$	$0.375 \pm 0.052$
LSTM	General	SPINN-GTD	<b><math>0.626 \pm 0.064</math></b>	$0.402 \pm 0.054$
CNN	Site Specific	Pure NN	$0.493 \pm 0.037$	$0.234 \pm 0.016$
CNN	Site Specific	SPINN-HEC18	<b><math>0.455 \pm 0.035</math></b>	<b><math>0.228 \pm 0.048</math></b>
CNN	Site Specific	SPINN-TD	<b><math>0.483 \pm 0.033</math></b>	$0.234 \pm 0.016$
CNN	General	Pure NN	$0.518 \pm 0.035$	$0.273 \pm 0.007$
CNN	General	SPINN-GTD	$0.525 \pm 0.026$	<b><math>0.259 \pm 0.015</math></b>
NLinear	Site Specific	Pure NN	$0.393 \pm 0.003$	$0.283 \pm 0.004$
NLinear	Site Specific	SPINN-HEC18	$0.396 \pm 0.003$	$0.284 \pm 0.007$
NLinear	Site Specific	SPINN-TD	<b><math>0.381 \pm 0.002</math></b>	<b><math>0.271 \pm 0.003</math></b>
NLinear	General	Pure NN	$0.488 \pm 0.004$	$0.243 \pm 0.002$
NLinear	General	SPINN-GTD	$0.490 \pm 0.003$	<b><math>0.243 \pm 0.001</math></b>

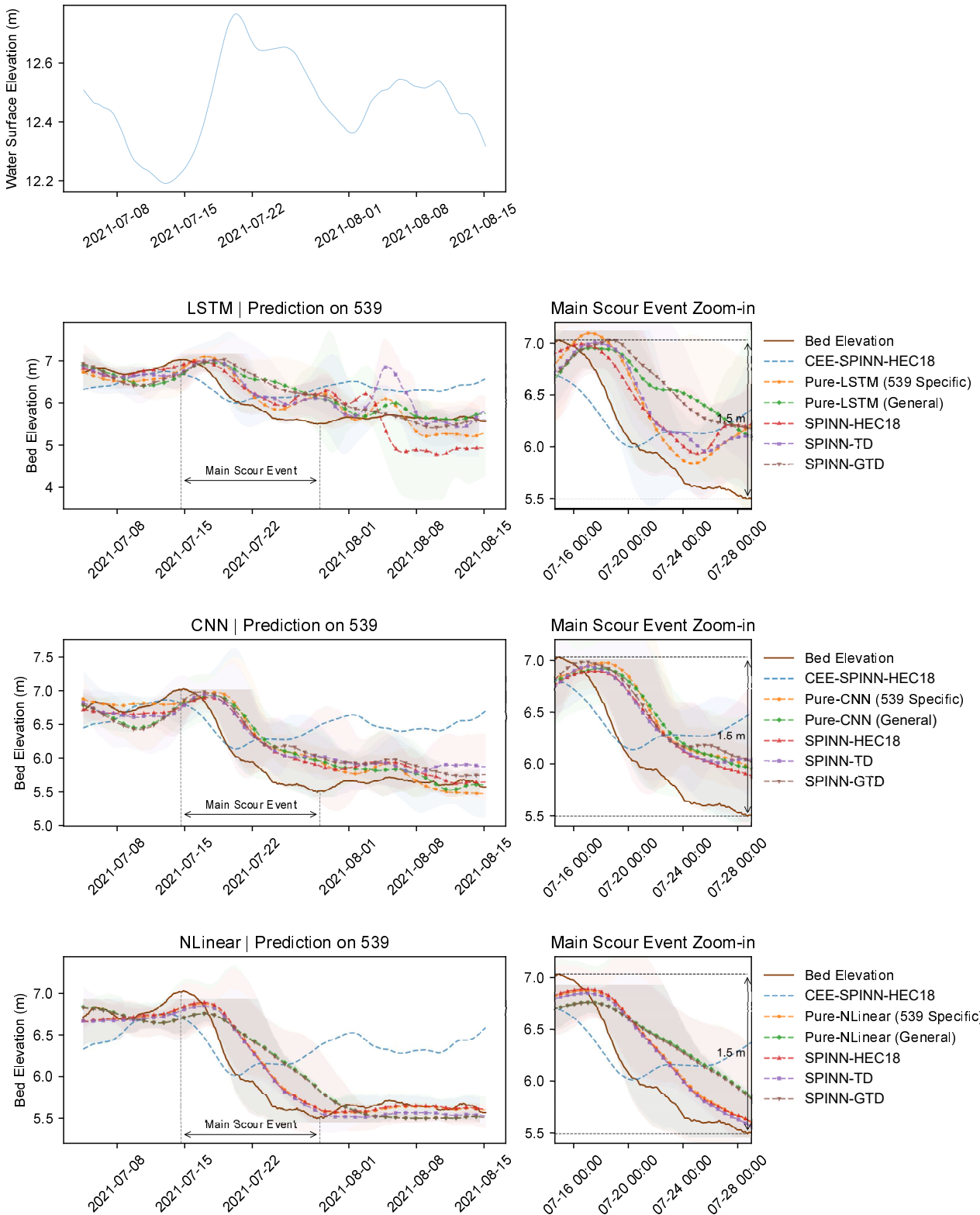


Fig. 10. Model predictions versus actual observations for Bridge 539 test set.

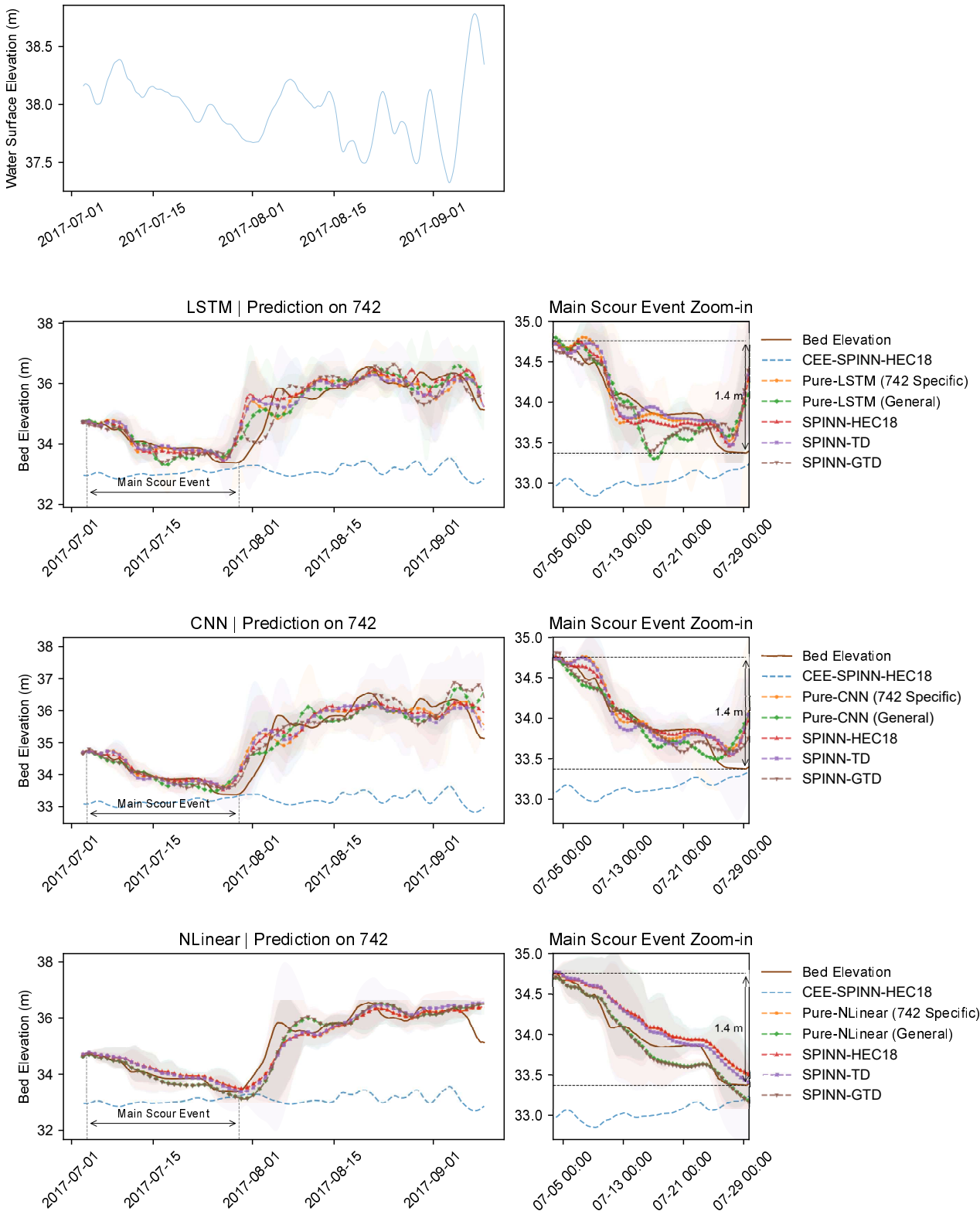


Fig. 11. Model predictions versus actual observations for Bridge 742 test set.

The site-specific pure NN models show varying performance across the LSTM, CNN, and NLinear groups. The LSTM-based models tend to show more fluctuations in predicting scour episodes, while the CNN and NLinear groups generally align more closely with actual scour trends.

The performance of SPINN variants varies depending on the base model and the specific bridge. For Bridge 539, the SPINN-TD variant shows slightly less error in scour depth prediction for CNN and NLinear base models (2.03% and 3.05%, respectively). The SPINN-HEC18 variant also enhances the performance of the CNN model, reducing the RMSE by 7.71%. In the case of Bridge 742, SPINN-HEC18 and SPINN-TD groups also show similar improvement but are not consistent for all base models.

The general data-driven and SPINN models often show larger errors in capturing trends of scour and filling compared to site-specific models. Only for Bridge 742, the SPINN-GTD variant demonstrated improved performance compared to the site-specific pure NN models when paired with the CNN and NLinear base models.

Comparing both data-driven and hybrid-physics-data-driven models with the calibrated HEC18 equation (CEE-SPINN-HEC18) shows the superiority of using dynamic DL models for scour prediction. This model struggles significantly in following the scouring and filling trends and significantly underestimating scour depth in most periods for both bridges 539 and 742 (see Figs. 10 and 11).

The performance of the models in capturing the major scour depth is generally consistent with their overall performance on the test dataset, as presented in Table A1. Minor differences in the relative performance of the models between the main scouring event (Table 8) and the overall test set (Table A1) can be attributed to the specific characteristics of the main scouring event and the model's ability to capture those particular patterns.

### 3.4 Calibrated Empirical Equations

This section focuses towards the calibrated empirical equations derived from the SPINN framework. We will evaluate the performance of the three calibrated equations (see Table 8) and assess their potential to be implemented as independent scour models.

Since the empirical equations are designed to predict maximum scour depth, their performance is only evaluated during scouring episodes. Bridge 539 paired with the NLinear group is chosen here as an example for detailed analysis, considering the deeper scouring depth and the superior performance of the base model.

Fig. 12 displays the training progress plots of the latent parameters incorporated in the three empirical equations over 500 training epochs. The parameter  $p_1$  in all equations acts as an overall adjustment factor, converging to distinct values for each equation, indicating its role in tailoring the output of each empirical equation. The  $p_2$  in HEC18 and TD, representing the adjustment on the velocity, stabilizes at 1.0 after initial training epochs, suggesting its impact may be mitigated by adjustments in  $p_1$ . Similarly,  $p_3$  in TD converges to 1.0, reflecting its minimal influence on the final results.  $T_L$ , the time lag of scour events, is calibrated to 1.95 and 2.35 hours in TD and GTD equations, respectively. This suggests the average time lag from start to stable scouring depth is around 2 hours for Bridge 539. Note that this length represents the average lag learned by the model, and it could be shorter or longer than particular cases. In the general model (GTD), the exponents  $\alpha$  and  $\beta$  display fluctuating convergence, indicating challenges in finding stable optimal values. The comprehensive summary of these calibrated parameters across different scenarios can be found in Table 9.

Fig. 13 compares the calibrated empirical equations (CEE) derived from the SPINN model for predicting maximum scour depth on the Bridge 539 test dataset. The actual bed elevation changes are highlighted with

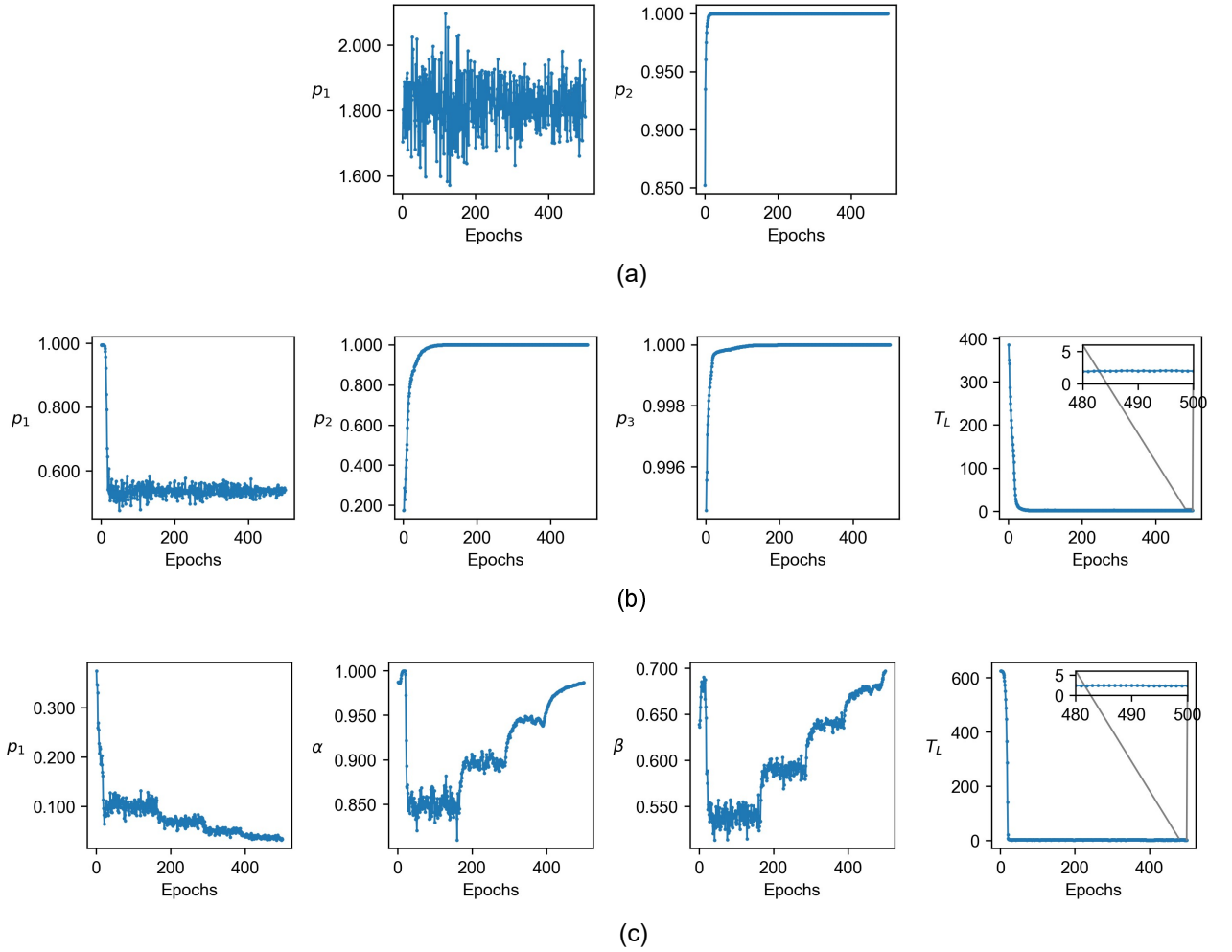


Fig. 12. The calibration of empirical equations with NLinear SPINN model, using the 539 dataset for site-specific models (GTD uses all datasets). a) The latent parameters of the HEC18 equation, b) The latent parameters of the TD equation, and c) The latent parameters of the GTD equation.

a solid brown line, while the predictions from the CEEs are marked with dashed lines. The CEE-SPINN-TD and CEE-SPINN-GTD employ time-dependent equations, where an exponential function predicts the scour depth for each timestep in the scouring episode. The predicted depth is zero at the beginning of the episode ( $t = 0$ ) and reaches the maximum scour depth ( $y_{s_{max}}$ ) at a time close to the calibrated time lag parameter ( $T_L$ ). Given the multi-step nature of the CEE-SPINN-TD and CEE-SPINN-GTD, each timestep within the scouring episode is predicted multiple times based on its sequential positioning. The dashed lines represent the mean of these multiple predictions, while the shaded areas denote the 95% confidence intervals. On the other hand, the CEE-SPINN-HEC18 (New  $E_{ref}$ ) uses the same dynamic reference level approach as the time-dependent equations to enable fair comparison. Since the CEE-SPINN-HEC18 (New  $E_{ref}$ ) does not have multiple predictions for each timestep, it has a single dashed line without uncertainty shades.

Among the CEEs calibrated through SPINN, the HEC18 shows difficulty in following the trends of scouring events and overestimates the maximum scour depth by up to 3 meters. As expected, GTD's

**Table 9.** The calibrated equation parameters from SPINN models.

Bridge	Equation	$p_1$	$p_2$	$p_3$	$T_L$ (hour)	$\alpha$	$\beta$
212	HEC18	2.49	1.0	N/A	N/A	N/A	N/A
212	TD	0.539	1.0	1.0	1.96	N/A	N/A
527	HEC18	0.524	1.0	N/A	N/A	N/A	N/A
527	TD	0.109	1.0	1.0	0.371	N/A	N/A
539	HEC18	1.78	1.0	N/A	N/A	N/A	N/A
539	TD	0.483	1.0	1.0	1.79	N/A	N/A
742	HEC18	1.34	1.0	N/A	N/A	N/A	N/A
742	TD	0.342	1.0	1.0	10.7	N/A	N/A
All	GTD	0.033	N/A	N/A	2.35	0.987	0.697

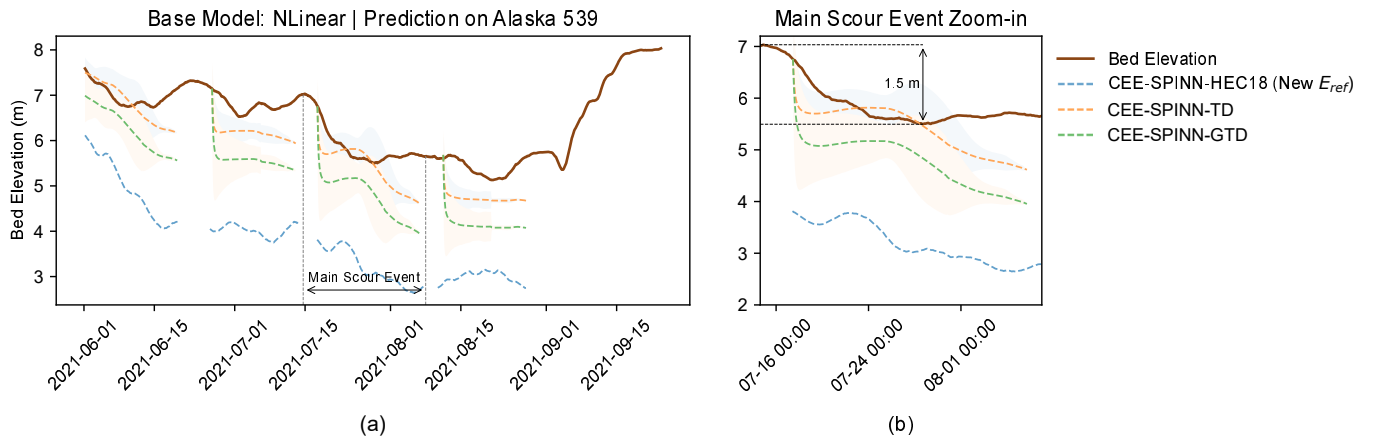


Fig. 13. a) Maximum scour prediction using the calibrated empirical models (CEE) for Bridge 539, b) magnified main scour episode.

performance is not as accurate as TD, which represents a site-specific version of the GTD model. During the main scouring event highlighted in Fig. 13b, the CEE-SPINN-HEC18, CEE-SPINN-TD, and CEE-SPINN-GTD yield RMSEs ( $m$ ) of 2.608, 0.562, and 1.096, respectively. While not as accurate as the SPINN models, these results demonstrate that the SPINN-calibrated time-dependent empirical equation can provide reasonable estimates of maximum scour depth with the advantage of much greater simplicity compared to the neural networks.

## 4 Conclusion

This paper introduced scour physics-informed neural network algorithms, SPINNs, exploring hybrid physics-data-driven models for bridge scour prediction based on deep learning. Central to SPINN's methodology is the integration of physics-based empirical equations as supplementary loss components into deep learning neural networks. We focused on three deep learning architectures, LSTM, CNN, and NLinear,

as base models for scour prediction. Both CNN and LSTM models have already proved competitive in real-time scour forecasts using historical monitoring data in our previous studies (Yousefpour and Correa, 2023; Hashem and Yousefpour, 2024). NLinear model was introduced for the first time for scour forecasting, demonstrating the highest accuracy and much lower computational cost compared to CNN and LSTM. Although SPINNs performance showed variability with the base DL model, the physics-based loss function/empirical equation, and the bridge-specific data, overall they showed superior performance in most forecasting scenarios/case studies compared to pure data-driven NN models. For some scenarios, such as the LSTM group in Bridge 539, the SPINN could help the base model reduce up to 50% forecasting error.

We explored the idea of generalised models for bridge clusters by aggregating bridge datasets in Alaska to train the DL models and use them for each specific bridge. The pure NN models mostly benefited from this approach. In particular, bridges with limited datasets achieved much more accuracy in predictions with the general models compared to site-specific ones. However, the general hybrid physics-data-driven models (SPINN-GTD) did not show superiority to site-specific physics-data-driven variants. We found that bridge-specific variants of SPINN, incorporating HEC18 and time-dependent (TD) empirical equations yield more accurate predictions compared to general time-dependent (GTD). The GTD empirical equation needs to adapt to a wide range of scour behaviour for a cluster of bridges during training, i.e., finding an optimal solution for latent parameters that are, in fact, bridge-specific. This can inadvertently limit the NN's ability to adequately learn and adapt to the specific scouring patterns in each particular bridge.

This study revealed that the sister calibrated empirical equations derived from SPINN, particularly the introduced time-dependent HEC18, can provide reasonable estimates of the maximum scour depth with potentially much higher accuracy than the traditional methods, such as HEC-18. As opposed to traditional HEC-18, which is often calibrated using discrete scour measurements, the empirical equations within SPINN are calibrated using historical time series scour monitoring data throughout the neural network training process. The generalised time-dependant calibrated equations can be particularly helpful in scenarios where site-specific bridge, flow and geology data are lacking, such as new bridge projects in a region.

Although the error reduction margins in scour predictions varied across different baseline models and bridges, SPINN framework proved to be an instrumental approach to improve scour prediction both in real-time forecasting and maximum scour depth estimation scenarios. Comparing the HEC18 model with SPINNs and pure DL models shows a significant improvement, which can benefit the current state of practice in bridge scour design and management.

## 5 Data Availability Statement

Some or all data used for this study are available from the corresponding author upon request. Models or codes generated or used during the study are proprietary or confidential in nature and may only be provided with restrictions. Related data and codes are available at <https://github.com/Data-Driven-Computational-Geotechnics/ScourSensePhase4/>.

## 6 Acknowledgments

This research was supported by The University of Melbourne’s Spartan and the GEO&CO Infrastructure HPC Center. The funding was provided by The University of Melbourne’s Start-Up awarded to Dr Negin Yousefpour.

## References

Amini, D., Haghishat, E., and Juanes, R. (2023). “Inverse modeling of nonisothermal multiphase poromechanics using physics-informed neural networks.” *Journal of Computational Physics*, 490.

Arneson, L., Zevenbergen, L., Lagasse, P., and Clopper, P. (2012). *Evaluating Scour at Bridges-Fifth Edition, Hydraulic Engineering Circular No. 18*. Federal Highway Administration (FHWA) (April).

Briaud, J.-L., Hurlebaus, S., Chang, K., Yao, C., Sharma, H., Yu, O.-Y., Darby, C., Hunt, B., and Price, G. (2011). “Real-time monitoring of bridge scour using remote monitoring technology.” *Rep. No. 0-6060-1*, Texas A&M University/TTI.

Briaud J.L., Medina-Cetina Z., Hurlebaus S., Everett M., Tucker S., Yousefpour N., and Arjwech R. (2012). “Unknown foundation determination for scour.” *Report no.*, Texas A&M University, College Station (8).

Chen, J. and Liu, Y. (2021). “Probabilistic physics-guided machine learning for fatigue data analysis.” *Expert Systems with Applications*, 168.

Chen, Y., Xu, Y., Wang, L., and Li, T. (2023). “Modeling water flow in unsaturated soils through physics-informed neural network with principled loss function.” *Computers and Geotechnics*, 161.

Eghbalian, M., Pouraghah, M., and Wan, R. (2023). “A physics-informed deep neural network for surrogate modeling in classical elasto-plasticity.” *Computers and Geotechnics*, 159.

Faroughi, S. A., Pawar, N. M., Fernandes, C., Raissi, M., Das, S., Kalantari, N. K., and Mahjour, S. K. (2024). “Physics-guided, physics-informed, and physics-encoded neural networks and operators in scientific computing: Fluid and solid mechanics.” *Journal of Computing and Information Science in Engineering*, 24.

Haghishat, E., Raissi, M., Moure, A., Gomez, H., and Juanes, R. (2021). “A physics-informed deep learning framework for inversion and surrogate modeling in solid mechanics.” *Computer Methods in Applied Mechanics and Engineering*, 379.

Hashem, T. and Yousefpour, N. (2024). “Application of long-short term memory and convolutional neural networks for real-time bridge scour forecast.

Hochreiter, S. and Schmidhuber, J. (1997). “Long short-term memory.” *Neural computation*, 9(8), 1735–1780.

Jia, X., Willard, J., Karpatne, A., Read, J. S., Zwart, J. A., Steinbach, M., and Kumar, V. (2021). “Physics-Guided Machine Learning for Scientific Discovery: An Application in Simulating Lake Temperature Profiles.” *ACM/IMS Transactions on Data Science*, 2(3).

Karniadakis, G. E., Kevrekidis, I. G., Lu, L., Perdikaris, P., Wang, S., and Yang, L. (2021). “Physics-informed machine learning.” *Nature Reviews Physics*.

Karpatne, A., Atluri, G., Faghmous, J. H., Steinbach, M., Banerjee, A., Ganguly, A., Shekhar, S., Samatova, N., and Kumar, V. (2017). “Theory-guided data science: A new paradigm for scientific discovery from data.” *IEEE Transactions on Knowledge and Data Engineering*, 29.

Kingma, D. P. and Ba, J. (2014). “Adam: A method for stochastic optimization.” *arXiv preprint arXiv:1412.6980*.

Kirby, A., Roca, M., Kitchen, A., Escarameia, M., and Chesterton, O. (2015). *Manual on scour at bridges and other hydraulic structures*. CIRIA.

Lan, P., jing Su, J., yan Ma, X., and Zhang, S. (2024). “Application of improved physics-informed neural networks for nonlinear consolidation problems with continuous drainage boundary conditions.” *Acta Geotechnica*, 19.

Li, K. Q., Yin, Z. Y., Zhang, N., and Li, J. (2024a). “A pinn-based modelling approach for hydromechanical behaviour of unsaturated expansive soils.” *Computers and Geotechnics*, 169.

Li, Y., Pan, Y., and Zhang, L. (2024b). “Physics-guided deep learning for driving force estimation in synchronous tunnel boring machines under missing cylinders.” *Automation in Construction*, 161.

Liang, B., Du, S., Pan, X., and Zhang, L. (2019). “Local scour for vertical piles in steady currents: Review of mechanisms, influencing factors and empirical equations.” *Journal of Marine Science and Engineering*, 8(1), 4.

Liu, M., Zeng, A., Chen, M., Xu, Z., Lai, Q., Ma, L., and Xu, Q. (2022). “Scinet: Time series modeling and forecasting with sample convolution and interaction.” *Advances in Neural Information Processing Systems*, 35, 5816–5828.

Livieris, I. E., Pintelas, E., and Pintelas, P. (2020). “A cnn–lstm model for gold price time-series forecasting.” *Neural computing and applications*, 32, 17351–17360.

Masi, F. and Einav, I. (2024). “Neural integration for constitutive equations using small data.” *Computer Methods in Applied Mechanics and Engineering*, 420.

Ngo, H. (2018). *Guide to bridge technology, part 8: hydraulic design of waterway structures*. Number AGBT08-18.

Paszke, A., Gross, S., Chintala, S., Chanan, G., Yang, E., DeVito, Z., Lin, Z., Desmaison, A., Antiga, L., and Lerer, A. (2017). “Automatic differentiation in pytorch.” *NIPS-W*.

Pei, T., Qiu, T., and Shen, C. (2023). “Applying knowledge-guided machine learning to slope stability prediction.” *Journal of Geotechnical and Geoenvironmental Engineering*, 149.

Pizarro, A., Manfreda, S., and Tubaldi, E. (2020). *The science behind scour at bridge foundations: A review*, Vol. 12.

Raiissi, M., Perdikaris, P., and Karniadakis, G. E. (2019). “Physics-informed neural networks: A deep learning framework for solving forward and inverse problems involving nonlinear partial differential equations.” *Journal of Computational Physics*, 378.

Sheppard, D. M., Demir, H., and Melville, B. W. (2011). *Scour at wide piers and long skewed piers*, Vol. 682. Transportation Research Board.

Tian, H. and Wang, Y. (2023). “Data-driven and physics-informed bayesian learning of spatiotemporally varying consolidation settlement from sparse site investigation and settlement monitoring data.” *Computers and Geotechnics*, 157.

Transportation Research Board (TRB) (2009). *Monitoring scour critical bridges*. NCHRP Synthesis of Highway Practice 396, Washington, D.C.

Vaswani, A., Shazeer, N., Parmar, N., Uszkoreit, J., Jones, L., Gomez, A. N., Kaiser, Ł., and Polosukhin, I. (2017). “Attention is all you need.” *Advances in neural information processing systems*, 30.

Venkatesan, R. and Li, B. (2017). *Convolutional neural networks in visual computing: a concise guide*. CRC Press.

Yousefpour, N. and Correa, O. (2023). “Towards an ai-based early warning system for bridge scour.” *Georisk: Assessment and Management of Risk for Engineered Systems and Geohazards*, 1–27.

Yousefpour, N., Downie, S., Walker, S., Perkins, N., and Dikanski, H. (2021). “Machine learning solutions for bridge scour forecast based on monitoring data.” *Transportation Research Record*, 2675(10), 745–

763.

Yousif, M. Z., Yu, L., and Lim, H. C. (2022). “Physics-guided deep learning for generating turbulent inflow conditions.” *Journal of Fluid Mechanics*, 936.

Yu, Y., Yao, H., and Liu, Y. (2020). “Structural dynamics simulation using a novel physics-guided machine learning method.” *Engineering Applications of Artificial Intelligence*, 96.

Zeng, A., Chen, M., Zhang, L., and Xu, Q. (2023). “Are transformers effective for time series forecasting?.” *Proceedings of the AAAI conference on artificial intelligence*, Vol. 37, 11121–11128.

Zhang, R., Liu, Y., and Sun, H. (2020). “Physics-guided convolutional neural network (phycnn) for data-driven seismic response modeling.” *Engineering Structures*, 215.

Zhou, H., Zhang, S., Peng, J., Zhang, S., Li, J., Xiong, H., and Zhang, W. (2021). “Informer: Beyond efficient transformer for long sequence time-series forecasting.” *Proceedings of the AAAI conference on artificial intelligence*, Vol. 35, 11106–11115.

Zhou, T., Ma, Z., Wen, Q., Wang, X., Sun, L., and Jin, R. (2022). “Fedformer: Frequency enhanced decomposed transformer for long-term series forecasting.” *International Conference on Machine Learning*, PMLR, 27268–27286.

Zhu, Y., Zabaras, N., Koutsourelakis, P. S., and Perdikaris, P. (2019). “Physics-constrained deep learning for high-dimensional surrogate modeling and uncertainty quantification without labeled data.” *Journal of Computational Physics*, 394.

## Appendix

**Table A1.** Comprehensive evaluation results of all experiments, comparing the performance of pure NN models and different SPINN variants across four bridge datasets.

Test Set	Base Model	Method	Physics-based Loss	Training Set (s)	Test MSE ( $m^2$ )
212	LSTM	Pure NN	N/A	212	$0.533 \pm 0.267$
212	LSTM	Pure NN (General)	N/A	All	$0.089 \pm 0.032$
212	LSTM	SPINN	HEC18	212	$0.443 \pm 0.350$
212	LSTM	SPINN	TD	212	$0.136 \pm 0.053$
212	LSTM	SPINN	GTD	All	$0.144 \pm 0.049$
212	CNN	Pure NN	N/A	212	$0.142 \pm 0.022$
212	CNN	Pure NN (General)	N/A	All	$0.101 \pm 0.032$
212	CNN	SPINN	HEC18	212	$0.150 \pm 0.039$
212	CNN	SPINN	TD	212	$0.173 \pm 0.044$
212	CNN	SPINN	GTD	All	$0.089 \pm 0.034$
212	NLinear	Pure NN	N/A	212	$0.010 \pm 0.001$
212	NLinear	Pure NN (General)	N/A	All	$0.013 \pm 0.000$
212	NLinear	SPINN	HEC18	212	$0.010 \pm 0.000$
212	NLinear	SPINN	TD	212	$0.010 \pm 0.000$
212	NLinear	SPINN	GTD	All	$0.013 \pm 0.000$
527	LSTM	Pure NN	N/A	527	$0.141 \pm 0.074$
527	LSTM	Pure NN (General)	N/A	All	$0.113 \pm 0.037$
527	LSTM	SPINN	HEC18	527	$0.135 \pm 0.091$
527	LSTM	SPINN	TD	527	$0.084 \pm 0.035$
527	LSTM	SPINN	GTD	All	$0.122 \pm 0.053$
527	CNN	Pure NN	N/A	527	$0.055 \pm 0.045$
527	CNN	Pure NN (General)	N/A	All	$0.123 \pm 0.021$
527	CNN	SPINN	HEC18	527	$0.040 \pm 0.013$
527	CNN	SPINN	TD	527	$0.050 \pm 0.024$
527	CNN	SPINN	GTD	All	$0.130 \pm 0.037$
527	NLinear	Pure NN	N/A	527	$0.019 \pm 0.000$
527	NLinear	Pure NN (General)	N/A	All	$0.049 \pm 0.001$
527	NLinear	SPINN	HEC18	527	$0.019 \pm 0.000$
527	NLinear	SPINN	TD	527	$0.023 \pm 0.000$
527	NLinear	SPINN	GTD	All	$0.049 \pm 0.001$
539	LSTM	Pure NN	N/A	539	$0.478 \pm 0.157$
539	LSTM	Pure NN (General)	N/A	All	$0.332 \pm 0.031$
539	LSTM	SPINN	HEC18	539	$0.388 \pm 0.078$
539	LSTM	SPINN	TD	539	$0.236 \pm 0.026$
539	LSTM	SPINN	GTD	All	$0.325 \pm 0.037$
539	CNN	Pure NN	N/A	539	$0.283 \pm 0.069$

539	CNN	Pure NN (General)	N/A	All	0.276±0.022
539	CNN	SPINN	HEC18	539	0.285±0.070
539	CNN	SPINN	TD	539	0.236±0.015
539	CNN	SPINN	GTD	All	0.250±0.022
539	NLinear	Pure NN	N/A	539	0.105±0.000
539	NLinear	Pure NN (General)	N/A	All	0.168±0.002
539	NLinear	SPINN	HEC18	539	0.105±0.002
539	NLinear	SPINN	TD	539	0.114±0.001
539	NLinear	SPINN	GTD	All	0.169±0.001
742	LSTM	Pure NN	N/A	742	0.884±0.589
742	LSTM	Pure NN (General)	N/A	All	0.325±0.021
742	LSTM	SPINN	HEC18	742	0.388±0.036
742	LSTM	SPINN	TD	742	0.260±0.021
742	LSTM	SPINN	GTD	All	0.346±0.045
742	CNN	Pure NN	N/A	742	0.214±0.037
742	CNN	Pure NN (General)	N/A	All	0.310±0.040
742	CNN	SPINN	HEC18	742	0.239±0.055
742	CNN	SPINN	TD	742	0.233±0.033
742	CNN	SPINN	GTD	All	0.335±0.024
742	NLinear	Pure NN	N/A	742	0.199±0.001
742	NLinear	Pure NN (General)	N/A	All	0.310±0.004
742	NLinear	SPINN	HEC18	742	0.200±0.002
742	NLinear	SPINN	TD	742	0.229±0.001
742	NLinear	SPINN	GTD	All	0.310±0.002

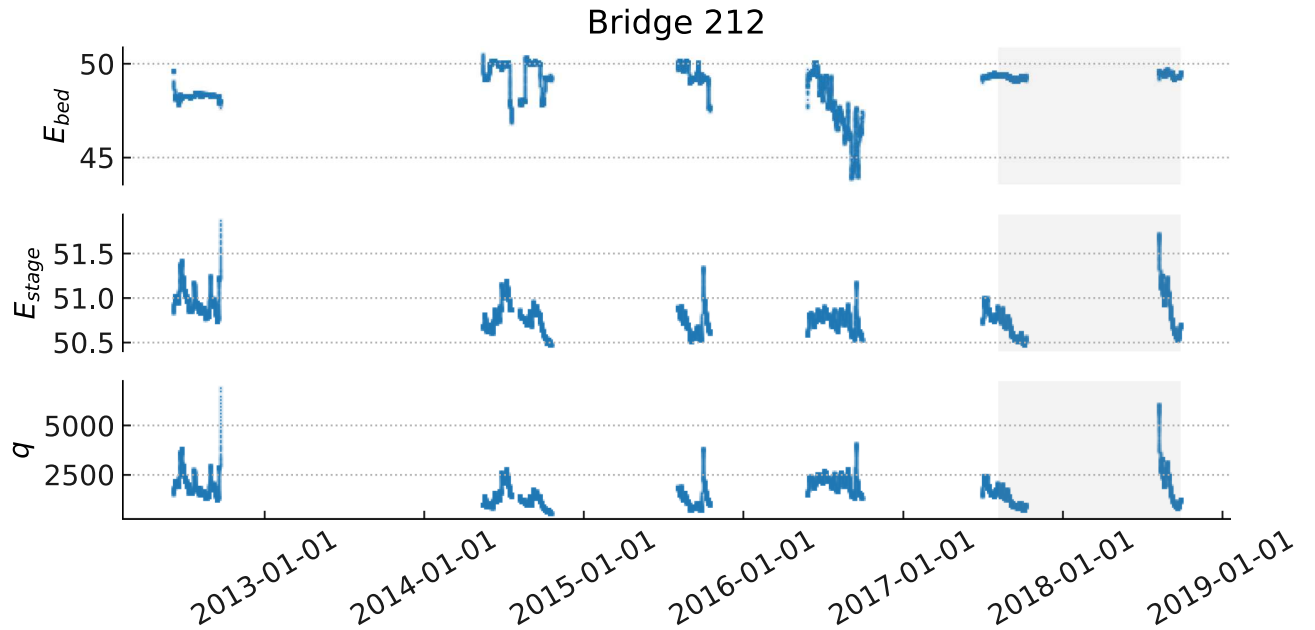


Fig. A1. Historical time series data for Bridge 212 shows the three features: bed elevation ( $m$ ), river stage elevation ( $m$ ), and discharge ( $m^3/s$ ). The grey zone shows the test subset, and the transparent part before is the training and validation subsets.

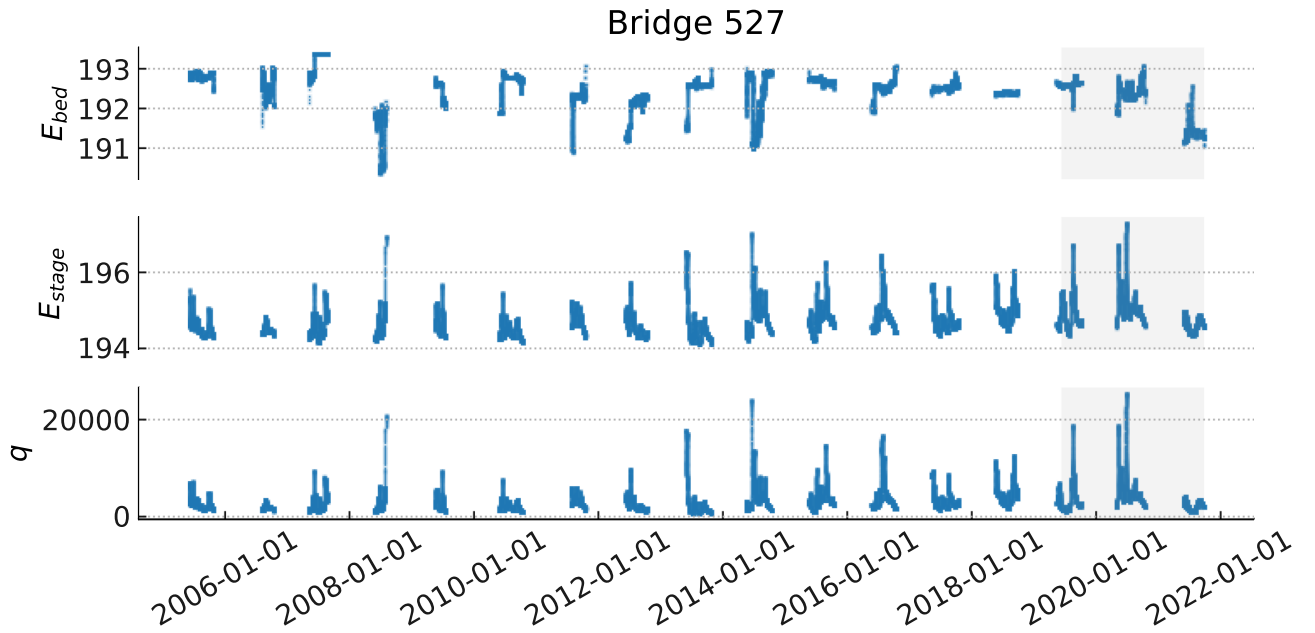


Fig. A2. Historical time series data for Bridge 527 shows the three features: bed elevation ( $m$ ), river stage elevation ( $m$ ), and discharge ( $m^3/s$ ). The grey zone shows the test subset, and the transparent part before is the training and validation subsets.

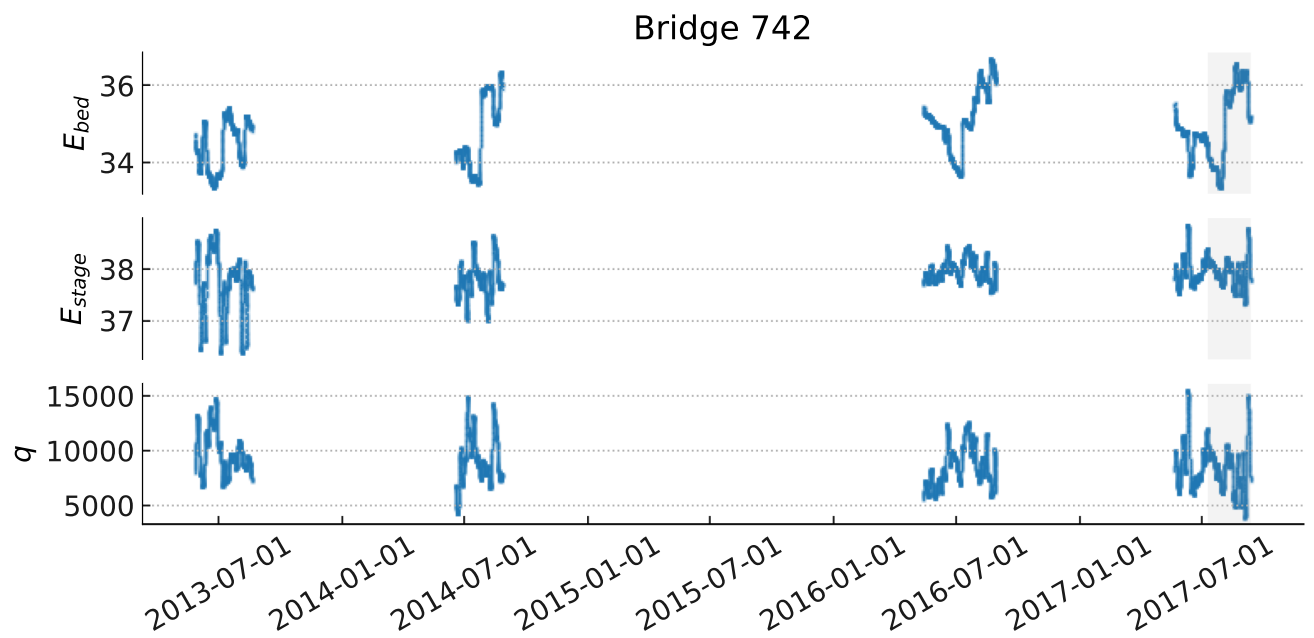


Fig. A3. Historical time series data for Bridge 742 shows the three features: bed elevation ( $m$ ), river stage elevation ( $m$ ), and discharge ( $m^3/s$ ). The grey zone shows the test subset, and the transparent part before is the training and validation subsets.